M.Sc. Engg. Thesis

MODELING AND DESIGN OF A MAGNETIC ANOMALY DETECTION SYSTEM FOR UNDERWATER SURVEILLANCE CONSIDERING STRATIFIED ISOTROPIC MEDIUM

by
Manik Dautta
Std. No: 1014062120

Submitted to

Department of Electrical and Electronic Engineering
Bangladesh University of Engineering and Technology (BUET)
Dhaka 1205, Bangladesh

August 2017

Dedication

To My Family

The dissertation entitled "**MODELING AND DESIGN OF A MAGNETIC ANOMALY DETECTION SYSTEM FOR UNDERWATER SURVEILLANCE CONSIDERING STRATIFIED ISOTROPIC MEDIUM**", submitted by Manik Dautta, Roll No: 1014062120, Session: October 2015, has been accepted as satisfactory in partial fulfillment of the requirement for the M.Sc. Engg. degree on August 12, 2017.

Board of Examiners

1. _____

Prof. Mohammad Ariful Haque — Chairman
Department of Electrical & Electronic Engineering — (Supervisor)
BUET, Dhaka 1205

2. _____

Head of the Department — Member
Department of Electrical & Electronic Engineering — (Ex-officio)
BUET, Dhaka 1205

3. _____

Prof. Md. Kamrul Hasan
Department of Electrical & Electronic Engineering — Member
BUET, Dhaka 1205

4. _____

Gp Capt Mohammed Hossam-E-Haider — Member
Professor and Head of the Department — (External)
Department of Electrical Electronic and Communication Engineering
MIST, Mirpur Cantonment, Dhaka 1216

Table of Contents

List of Figures

List of Tables

Acknowledgments

I would love to express my heartiest gratitude to my supervisor Dr. Mohammad Ariful Haque, Professor, Department of Electrical and Electronic and Engineering, Bangladesh University of Engineering and Technology (BUET), Dhaka.His supervision, encouragement and personal guidance were always with me during the progress of the thesis. His concepts and problem solving approach have been very helpful for the successful completion of this work. I am ever grateful to him.

My thanks and appreciations go to 'Anyeshan Limited', which is a non-profit research organization, for it's financial and research resources support to me. I am also thankful to all of my teachers and colleagues who have willingly helped me out with their busy schedule.

Finally, and most importantly, I remember my parents and family members, specially my wife, who are always a source of inspiration in every good action. I am grateful to them for their faith in me and allowing me to be as ambitious as I wanted. It was under their watchful eye that I gained so much drive and an ability to tackle challenges head on.

Abbreviations

EM - Electromagnetic

EMD - Empirical Mode Decomposition

HMD - Horizontal Magnetic Dipole

IMF - Intrinsic Mode Function

MAD - Magnetic Anomaly Detection

NSL - Noise Source Layer

PF - Particle Filter

UKF - Unscented Kalman Filter

UAV - Unmanned Aerial Vehicle

VMD - Vertical Magnetic Dipole

μ - Magnetic Permeability of the Medium

ε - Electric Permittivity Of the Medium

σ - Electric Conductivity of the Medium

B - Magnetic Flux Density

H - Magnetic Flux Intensity

Abstract of the Thesis

This thesis presents a method of underwater surveillance of ferromagnetic objects based on Magnetic Anomaly Detection. A numerical method of calculating electromagnetic fields produced by the elementary dipole sources in a stratified media is built. The method is useful in estimating magnetic signature at the air generated by the ferromagnetic objects submerged in the ocean. Mathematical modifications to match the same method for a means of measuring magnetic noise signals where noise sources are modeled as multiple equivalent electric and magnetic dipoles distributed at the environment are developed. After developing the simulation environment which is aimed at mimicking the real ocean environment, Empirical Mode decomposition technique is used to anlyse the noisy magnetic signals recorded by Tri-axial magnetometer from Unmanned Aerial Vehicle. It decomposes the obtained signals into Intrinsic Mode Functions and Residue, and responds to any anomaly found in the denoised signals. A Triangular geometry of sensor positions is proposed with combined Particle Filter and Unscented Kalman Filter as signal processing algorithms for the classification, localization and tracking of the target in this study.

Chapter 1

INTRODUCTION

1.1 Motivation

The exploration of the ocean is far from being complete, and it enables research and applications in many different areas with scientific, cultural or industrial interest, such as unexploded ordnance (UXO) detection, underwater buried mine hunting, underwater vessel detection, archeologic survey, geologic prospecting, or biomedical applications, to name but a few. Again many of these tasks that were originally achieved with towed arrays or manned vehicles are being completely automated, as a result of advancements in the efficiency, size, and memory capacity of computers with the help of Autonomous Underwater Vehicle (AUV), Remotely Operated Vehicle (ROV), Unmanned Underwater Vehicle (UUV).

Due to the necessity of the recent defense strategies, the monitoring, control and navigation of these unmanned vehicles are of great interests in underwater surveillance system. Methods of detecting targets include sonar, radar, electronic support measures, and magnetic anomaly detection. It has predominantly been performed by sonar technologies i.e. forward-scan sonar, sonar imagery, multi beam forward-looking sonar images, MIMO sonar [1, 2, 3], and in few cases by optical method i.e. laser and optical imaging [4, 5, 6]. But some shortcomings such as limitations at the signal transmission due to small bandwidth and low data

rate, high latency and variable sound speed due to fluctuating water temperature and salinity, signal corruption and scattering due to reverberation, multi-path propagation, and complex flow pattern of the water coupled with the presence of an upper (free surface) and lower (sea bottom) boundary, made the performances of the acoustics based system unreliable. Similarly, limited on-site accessibility, poor signal acquisition control, insufficient illumination and wavelength-dependent light absorption, modification of the intrinsic parameters due to air-water interface, scattering and light diffusion, cause the unsatisfactory results of optical systems.

Light, radar, or sound energy cannot pass from air into water and return to the air in usable level for airborne detection. The lines of force in a magnetic field are able to make this transition almost undisturbed, however, because magnetic lines of force pass through both water and air in similar manners. Owing to these advantages, use of electromagnetic (EM) waves is on rise. One of the several techniques is Magnetic Anomaly Detection (MAD) system which senses the anomaly in earth magnetic field produced by the ferromagnetic objects. In recent years, the latest magnetic sensors have already achieved a very high accuracy, for instance, the optically pumped magnetometer and the superconducting quantum interference magnetometer have reached an accuracy level of pT and even fT. This actually provides a new chance to realize the high-accuracy real-time surveillance based on EM techniques. So, working on MAD system is interesting, challenging and worth to explore.

1.2 Challenge of Designing MAD System

The challenges of designing a MAD system are:

- The air-water interface makes the computation of EM fields is a complex

problem for airborne surveillance of underwater ferromagnetic objects like Unmanned Aerial Vehicle (UAV) based MAD system.

- The suppression of environmental electromagnetic noise or the mitigation of its effects from myriad of interfering sources on the measured signals is a major concern.

- Magnetic signal varies with target magnetization related to the target size, properties of the medium and the distance between the target and the sensor position. So, simultaneous optimization between target magnetization and distance is a great challenge.

- For a good surveillance system, low False Alarm Rate (FAR) and large operating area, along with physical parameters, kinematic parameters are also important. So, state vector should include velocity, which has to be determined for continuous tracking of the target.

1.3 Contribution of the Thesis

This thesis deals with problem of the performance of the MAD system which is governed by the complexity of underlying electromagnetic processes. Due to high attenuation of EM signal, as complex permittivity and conductivity of the seawater are high, the signal to noise ratio (SNR) of the recorded signal is low. Our contribution in this study are:

- We develop an environment which is aimed at mimicking the salient magnetic features of the ocean environment encountered by the MAD sensor for a

specified location and for a set of realizable ocean conditions and geographical topologies.

  - We propose an elegant computational technique for measuring the EM fields in three layered stratified media.
  - After developing a simple model to calculate the induced magnetization of the ferromagnetic target due to external earth's magnetic field, this technique can be used for observing the magnetic anomaly produced by the target.
  - A volumetric distribution of isolated elementary multiple dipoles having random magnetic moments, orientations and frequencies are considered as sources of magnetic noise for MAD system. A generic mathematical model is developed to generate the ocean induced low frequency electromagnetic noises for practical ocean environment.

- Tri-axial magnetometers are incorporated in an UAV based MAD sensor to obtain the signals. Empirical Mode Decomposition (EMD) method is used to decompose the signal into Intrinsic Mode Functions (IMFs) and Residue, and to response to the anomalies if found.

- We propose combined Particle Filter (PF) and Unscented Kalman Filter (UKF) in Triangular 3-sensor geometry for simultaneous target classification, localisation and tracking.

1.4 Outline of the Thesis

The rests of the thesis are organised as follow:

Chapter 2 describes the working principle of a MAD system and previous works on related underwater surveillance using magnetic field measurement. Different techniques has been proposed to monitor the ocean activities for many years but the problem still requires more demonstrations.

Chapter 3 presents a generic mathematical model which is used to design the signal generation system considering air-ocean environment as a three layered (air, seawater, seabed) stratified media. Section 3.1 includes model for calculating EM fields due to a single dipole in a stratified media, Section 3.2 shows the model for measuring target magnetization in earth's magnetic field and Section 3.3 shows the modification of the model of Section 3.1 for calculating EM fields for multiple isolated elementary dipoles.

Chapter 4 describes the Empirical Mode Decomposition (EMD) techniques for decomposing the signal into Intrinsic Mode Functions (IMFs) and Residue. A MAD sensor moving in the air, equipped with a three-axis magnetometer, is used to denoise the signals from IMFs, and to response to any anomaly found in the observed low frequency noisy magnetic fields. It also includes the system modeling as state space dynamics, and brief description of Unscented Kalman Filter (UKF) and Particle Filter (PF) which are used to estimate the target's magnetic moment, and target's motion parameter i.e. position and velocity of the target. A Triangular 3-sensors and Pyramid 5-sensors system are used for the investigation of better estimation of the target parameters instead of conventional Linear 2-sensors system.

Chapter 5 presents performance evaluation of the proposed MAD system. Few representative numerical results are shown as magnetic noise signals for a few realizations out of an ensemble of possible realizations of elementary dipole source distributions. After that EMD techniques are used to detect hidden anomaly

produced by the target. Then filtering techniques are used for target classification, localization and tracking. Some simulations are shown for known magnetic moment as it has some specific applications also.

Finally, some concluding remarks of our task and also the scopes of future works are included in Chapter 6.

Chapter 2

WORKING PRINCIPLE OF A MAD SYSTEM AND LITERATURE REVIEW

2.1 Working Principle of a MAD System

A MAD system, usually mounted on an UAV, is able to confirm the detection, and accomplish classification, localization and tracking of large ferromagnetic objects submerged in an ocean environment. MAD system uses the principle that ferromagnetic objects disturb the magnetic lines of force of the earth. These lines of force are able to pass through both water and air in a similar manners. Distortion of the earth magnetic field due to ferromagnetic body is shown in Figure 2.1. View A, shows the angular direction at which natural lines of magnetic forces enter and leave the surface of the earth. View B represents an area of undisturbed natural magnetic field. In views C and D, target's magnetic field distorts the natural field. The density of the natural field is decreased in view C, and increased in view D. This distortion can be used to detect the underwater objects.

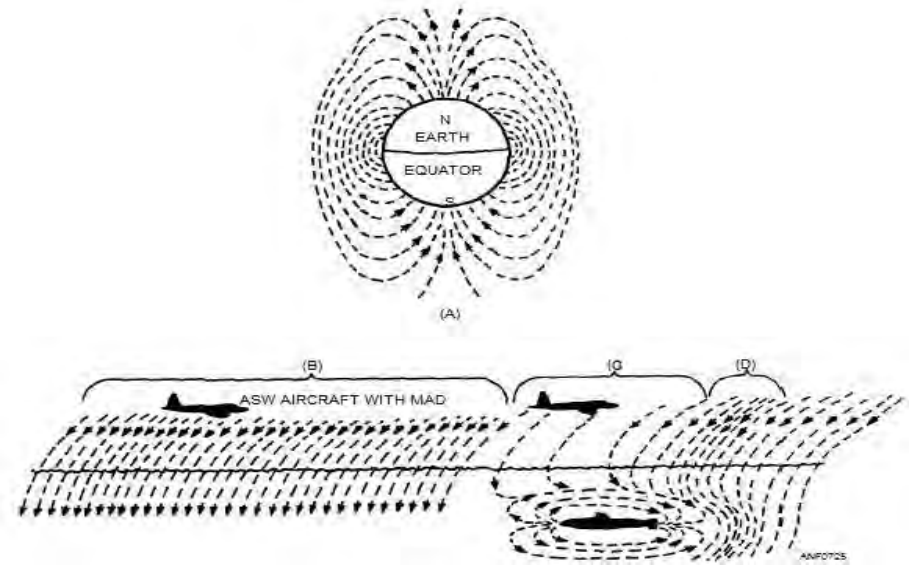

Figure 2.1: Distortion of the Magnetic Field

A MAD sensor in a MAD-equipped UAV responds to temporally- and spatially-varying earth's magnetic field, magnetic noise generated by the UAV, ocean-induced magnetic noise, geomagnetic noise, magnetic noise caused by local geological features, magnetic signals generated by ferromagnetic wreckage on the ocean floor, and the magnetic signal produced by the ferromagnetic target.Among these, the desired signal is the target signal or the target signature.It depends on target's altitude and size, shape, internal structure, material composition, depth, instantaneous velocity, motion-induced eddy currents, and corrosion-related sources [7]. Figure 2.2 illustrates the myriad of sources of magnetic fields that contribute to the total signal received by the MAD sensor. The list of sources is not exhaustive, but is intended to demonstrate the complex structure of magnetic signals.

Figure 2.2: Schematic of Sources of Magnetic Fields

The physical and kinematic components of the ferromagnetic body that impact the target signature will be collectively referred to as target parameters. The process of separating the unwanted components termed as noise, from the signal of interest is known as denoising. From the denoised signals detection of the target can be done based on the presence of any magnetic anomaly. Estimation of the magnetic moment of the target is called classification while localisation means estimating the initial position of the target. The tracking is the determination of velocity for continuous monitoring of the moving target along the trajectory. Our task will be to detect small target signals in the midst of interfering magnetic signals, as well as to estimate the target parameters for target classification, localisation and tracking.

2.2 Literature Review

2.2.1 Brief Description of Dominant Noises Sources

Environmental noise can be a major limitation on the performance of the magnetic sensor. EM fields and their gradients in electrically conductive seawater are distorted by myriad of interfering signals produce from different noise sources in the ocean environment. The power spectra of some of these components are affected by the search speed via Doppler shift. Such shifts are sometimes advantageous since they could elevate certain noise-power to frequencies greater than those relevant for detection. But in this documents Doppler effects are not considered. Here the sources and nature of dominant magnetic signals that contribute to the signal received by the MAD system are highlighted.

Ocean-induced magnetic noise

The ocean is an electrically conducting fluid that generates secondary magnetic fields as it flows through the earth's main magnetic field [8]. Additionally, the electromagnetic field generated by a progressive ocean wave contains a transverse magnetic type field due to seawater velocity components found in the vertical plane containing the direction of wave propagation [9, 10]. At sea level, magnetic signal strength due to ocean current and eddies can each be as large as few nT [11].

Geomagnetic noise

One of the major magnetic noises is the geomagnetic noise in the $0.0001 - 2Hz$ frequency band. It originates from the currents in the ionosphere, caused

by the interaction of solar wind particles with the earths magnetic field.Such geomagnetic noise has a Gaussian distribution with a root-mean-square (rms) value of approximately $0.3nT$.

Magnetic noise due to local geological features

Besides the earth's magnetic field, the most important magnetic field in the sea is the field created by remnant and induced magnetization in the rocks and sediments of the sea bottom. The field arising from magnetic materials in the earth's crust varies on all spatial scales and is often referred to as the anomaly field [12].

Magnetic noise from UAV

Magnetic detection from a UAV becomes an even more challenging task because of interfering magnetic signals originating from the UAV platform. The insulating materials that enclose the sensors and their associated electronics, which must be taken into account so that underwater measurements by sensors that have been calibrated in air can be corrected. Classic sources of magnetic noise include the fields produced by the UAV's permanent, induced, and eddy current magnetic moments. Electronic sources of noise include those produced by the UAV's avionics, wiring, and power generation/supply. UAV noise may at times overwhelm typical MAD signals if left uncompensated. The static part of the noise can be easily calibrated and subtracted from sensor readings. However, it is more difficult to characterize the dynamic magnetic effects of actions, such as the changing engine RPM.

Temporal variation of earth's magnetic field

The intensity and structure of the earth's magnetic field are constantly changing, slowly but erratically, reflecting the influence of the flow of thermal currents within the iron core. This variation is reflected in part by the wandering of the North and South Geomagnetic Poles. However, given the roughly five-year cycle of variation in the earths magnetic field, we can safely ignore its negligible effects.

So, the mapping of the magnetic noise is an essential part of the MAD system design. A model is necessary to generate the magnetic noise field considering the specific ocean nature. In this study we present an elegant computational technique which is developed to produce magnetic noise fields for a set of realizable ocean conditions due to different noise sources modeled as equivalent electric and magnetic dipoles. Noise generated by this model can be used to test the effectiveness of any system at different noisy environments.

2.2.2 Recent Trend in Surveillance Systems

Present defense strategy requires the continuous monitoring of the activities of surface and underwater objects in a certain area. This surveillance is waged by surface, airborne, undersea, and shore-based forces, each with its own unique capabilities. In this study the surveillance system that allows target detection, classification, localization and trajectory tracking based on magnetic data has been exploited.

Generally two main kinds of magnetic sensors are used to measure the magnetic fields in the MAD sensor platforms: magnetometers and gradiometers. Magnetometers measure the local magnetic field while some of them only measure

the magnitude of the magnetic field (scaler magnetometers), other measure the field components (vector/tri-axial magnetometers). Gradiometers measure the gradient of the magnetic field and are therefore less sensitive to slowly varying magnetic field (geologic or geomagnetic noise) than magnetometers.

As extremely low frequency components are dominant in both target signal and ocean induced EM noise signal, Fourier and spectral analysis are not adequate for exploring the hidden desired signals from recorded noisy signals. A representative three layered (air-seawater-seabed) geometry having moving magnetic sensor platform in air, a large ferromagnetic target in water, myriad of noise sources modeled as equivalent electric and magnetic dipoles is shown in Fig. 2.3, which is used in UAV based MAD system for searching the magnetic anomaly produced by the target.

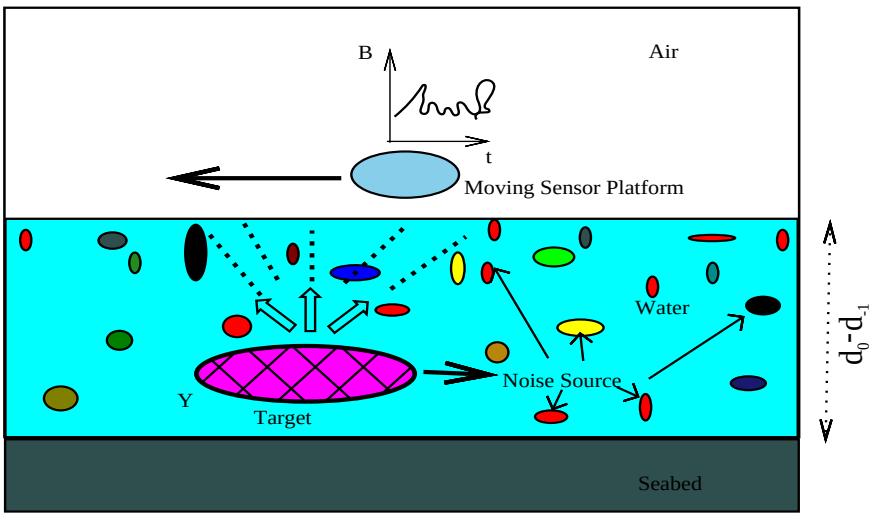

Figure 2.3: Schematic View of a Detection System

Some methods have been reported in different studies to detect the target from

observed noisy magnetic anomaly signals. The detection of a moving ferromagnetic target using a static three-axis referenced magnetometer can be done where the signal is decomposed into a set of orthonormal basis functions, out of which the dominant basis function is chosen as the detector. The recorded signals of magnetic sensors are transformed into energy signals to improve SNR as a part of target detection by using the set of orthogonal basis functions [13, 14]. Here detection is done for small magnetic dipole ($1Am^2$) at a very close distance ($7m$) from the observation point using Z-fluxgate which contain bell shaped signal. Whereas practically the signal can be any shape and target may be of small to large magnetic dipole at a large distance from the MAD sensor depending on the mission. Wavelet thresholding is another signal estimation technique that exploits the capabilities of wavelet transformation for signal denoising. It removes noise by killing coefficients that are insignificant relative to some data dependent threshold, and turns out to be very simple and effective. But use of magnetic maps in Automated Wavelet Detection (AWD) where accurate estimation of sensor location is essential for non-linear inversion method. The errors propagate from one step to the next resulted in a highly fluctuating estimation in the presence of noise [15, 16]. Another common way to detect a magnetic target is to look at the maxima of the magnitude of the magnetic field gradient (sometimes called 3D analytic signal amplitude). Most of the time, the maximum of this quantity is located approximately above the target [17, 18]. This signal exhibits maxima over magnetization contrasts, independent of the ambient magnetic field and source magnetization directions. So only under the assumption that the anomalies are caused by vertical contacts, the analytic signal is used to estimate depth which is not true in every case. A linear Euler deconvolution technique is also used in some studies to detect a dipole source where deconvolution

is done to the measured fields of three-axis gradiometers. It does not require grid interpolation, and any initial estimation of the parameters [19, 20]. But detection is highly depended on the structural index which is related to the geometry of the source. Incorrect choice of structural index leads to errors in estimated source depths. So, a successful detection system should detect objects having different shapes and sizes, from small to large magnetic moment at small to large distance, and most importantly in a highly noisy environment.

When detection is done, it is necessary to classify, localise and track the the target.Different approaches such as optimization algorithms namely Genetic Algorithm (GA) [13, 14], Particle Swarm Optimization (PSO) [21], numerical methods like potential field inversion method [22], linearization of non-linear functions [23], successive filtering window [24], magnetic maps, superconducting quantum interference devices(SQUIDs) [25] etc., are investigated for this purposes. GA and PSO are used to find the most possible solution of the search space. But some problems of these optimization techniques as they do not guarantee an optimal solution, the stop criterion is not clear, they do not use the gradient of the problem being optimized, make the use of them limited. Ginzburg used statistical mean of 100 executions of GA to have the desired result close to true parameters [13, 14]. Fan conducted a simulation experiments using scalar magnetometer array and particle swarm optimization (PSO) algorithm where the quality of the solution calculated is not too high as PSO algorithm can't jump out from the local optima when trapping in it [21].The performance of SQUIDs depends on having a "clean", isolated dipole signature [25], while only the background of smooth geomagnetic field and geomagnetic anomalies are considered by Jun [23]. The second-horizontal derivative anomalies obtained from magnetic data with filters of successive window

lengths used for classification and depth measurement but the data produced by simple geological structures and with a sensor array designed scan routine (scan along several lines) [24].

As the magnetic field measurement in this task is the non-linear function of the different target parameters, simultaneous classification, localisation and tracking is a complex problem. It requires iterative simulations of the parameters.

Chapter 3

MATHEMATICAL MODEL DEVELOPED FOR SIGNAL GENERATION

The environment for UAV based MAD system is considered as a three layered isotropic media (air-seawater-seabed) in this study, where UAV moves in air to measure the magnetic field produced by magnetic objects submerged in seawater. The geometric configuration of that method for three different regions are described in Fig. 3.1. Here for sea-water environment region (1) is air, region (0) is seawater and region (-1) is seabed plane. Point P is the observation point at air, and the target is located in seawater at the origin of the coordinate. $d_0 - d_{-1}$ represents width of the seawater region, where d_0 is the distance from the target to the air-seawater interface and d_{-1} is the distance from the target to the seawater-seabed interface. In the following parts of this chapter, mathematical models are developed to generate the signals received by the MAD sensor.

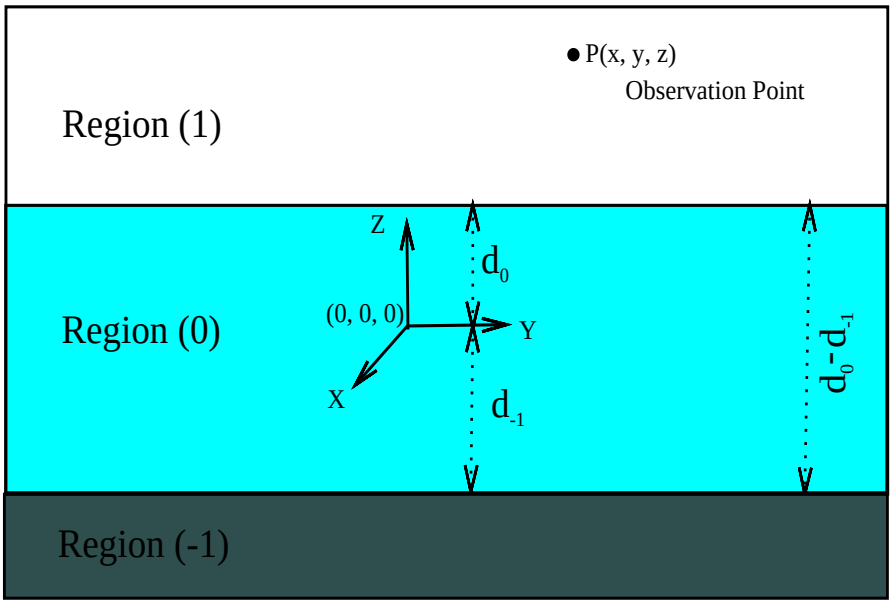

Figure 3.1: Geometric Representation of a Three Layered Media

3.1 COMPUTATION OF MAGNETIC FIELD IN A LAYERED MEDIA

For a magnetic dipole having moment vector $\tilde{\mathbf{m}}$, magnetic flux density $\tilde{\mathbf{B}}$ in an uniform medium is given as,

$$\tilde{\mathbf{B}}_{mdip}(\mathbf{r},\omega) = \frac{\mu}{4\pi}\left[\frac{k^2(\hat{r}\times\tilde{\mathbf{m}})\times\hat{r}}{r} + \{3\hat{r}(\hat{r}\cdot\tilde{\mathbf{m}}) - \tilde{\mathbf{m}}\}\left\{\frac{1}{r^3} - \frac{ik}{r^2}\right\}\right]e^{ikr} \qquad (3.1)$$

Here, Time dependence $e^{-i\omega t}$ is assumed. Position vector of the observation point with respect to dipole position is $\mathbf{r}$, unit vector along the direction of $\mathbf{r}$ is $\hat{r}$, magnetic permeability of the medium is μ, wave number which denotes phase change per meter for a wave is $k = \omega\sqrt{\mu\varepsilon'}$, complex permittivity of the medium which depends on

the frequency and electric conductivity of the medium is $\varepsilon' = \varepsilon + i\frac{\sigma}{\omega}$.

In case of a stratified anisotropic media, a method is presented for calculating EM fields by Tang in Ref. [26]. A ferromagnetic target can be adequately modeled at a distance by an equivalent magnetic dipole moment. The dipole source can be horizontal electric dipole, horizontal magnetic dipole, vertical magnetic dipole, or vertical electric dipole. The magnetic field intensity is expressed in TE (Transverse Electric) and TM (Transverse Magnetic) modes as,

$$\tilde{\mathbf{H}} = \tilde{\mathbf{H}}^{TM} + \tilde{\mathbf{H}}^{TE} \tag{3.2}$$

In region (j) the general solutions for waves outgoing in the $\hat{r}$ direction and travelling in the $\hat{z}$ direction for a single dipole placed at the origin of the coordinate are listed below. TM components are:

$$\tilde{\mathbf{H}}_j^{TM} = \overline{H}_j^{TM}(r)\,\hat{e}_r + \overline{H}_j^{TM}(\phi)\,\hat{e}_\phi + \overline{H}_j^{TM}(z)\,\hat{e}_z$$

$$\tilde{\mathbf{H}}_j^{TM} \begin{cases} r \\ \phi \\ z \end{cases} = \begin{cases} \int_{-\infty}^{+\infty} d\lambda \left(\frac{-i\omega\varepsilon'_j}{\lambda^2 r} \alpha_j^+(\lambda, z)\, H_n^{(1)}(r\lambda)\, S_n^{TM\prime}(\phi) \right) \\ \int_{-\infty}^{+\infty} d\lambda \left(\frac{i\omega\varepsilon'_j}{\lambda} \alpha_j^+(\lambda, z) H_n^{(1)\prime}(r\lambda)\, S_n^{TM}(\phi) \right) \\ 0 \end{cases} \tag{3.3}$$

Whereas TE components are:

$$\tilde{\mathbf{H}}_j^{TE} = \overline{H}_j^{TE}(r)\,\hat{e}_r + \overline{H}_j^{TE}(\phi)\,\hat{e}_\phi + \overline{H}_j^{TE}(z)\,\hat{e}_z$$

$$\tilde{\mathbf{H}}_j^{TE} \begin{cases} r \\ \phi \\ z \end{cases} = \begin{cases} \int_{-\infty}^{+\infty} d\lambda \left(\frac{-\gamma_j{}^{(m)}}{\lambda} \beta_j^-(\lambda, z) H_n^{(1)\prime}(r\lambda)\, S_n^{TE}(\phi) \right) \\ \int_{-\infty}^{+\infty} d\lambda \left(\frac{-\gamma_j{}^{(m)}}{\lambda^2 r} \beta_j^-(\lambda, z) H_n^{(1)}(r\lambda)\, S_n^{TE\prime}(\phi) \right) \\ \int_{-\infty}^{+\infty} d\lambda \left(\beta_j^+(\lambda, z) H_n^{(1)}(r\lambda)\, S_n^{TE}(\phi) \right) \end{cases} \tag{3.4}$$

Here,

$$\gamma_j{}^{(e)} = \sqrt{\lambda^2 a_j - k_j^2}, \quad a_j = {\varepsilon_j{}'}/{\varepsilon_{z,j}{}'}$$

$$\gamma_j{}^{(m)} = \sqrt{\lambda^2 b_j - k_j^2}, \quad b_j = {\mu_j}/{\mu_{z,j}}$$

$$\begin{aligned} \alpha_j{}^{\pm}(\lambda, z) &= \pm A_j(\lambda)\, e^{\gamma_j{}^{(e)} z} + B_j(\lambda)\, e^{-\gamma_j{}^{(e)} z} \\ \beta_j^{\pm}(\lambda, z) &= \pm C_j(\lambda)\, e^{\gamma_j{}^{(m)} z} + D_j(\lambda)\, e^{-\gamma_j{}^{(m)} z} \end{aligned} \tag{3.5}$$

From Equations (3.3) and (3.4), the first, second and third elements of the column matrices are the $\hat{r}$, $\hat{\phi}$ and $\hat{z}$ components of the field in cylindrical coordinate system respectively. Primes on any term denotes differentiation with respect to the arguments. For isotropic media, $a_j = 1$, $b_j = 1$. $H_n^{(1)}$ is the Hankel function of the first kind of the order n. For small argument $r\lambda$,

$$\lim_{\lambda \to 0} H_1^{(1)}(r\lambda) = \lim_{\lambda \to 0} \left[\frac{-2i}{\pi r \lambda} + \left\{ \frac{1}{2} \frac{i\left(-1 + 2\Gamma - 2\ln 2 + 2\ln(r\lambda)\right)}{2\pi} \right\} r\lambda + O\left(r\lambda^3\right) \right] \tag{3.6}$$

and the first derivative is,

$$H_n^{(1)'}(r\lambda) = {nH_n^{(1)}(r\lambda)}/{(r\lambda)} - H_{n+1}^{(1)}(r\lambda) \tag{3.7}$$

$A,\ B,\ C,\ D$ depend on λ and have determined by solving boundary conditions. For region (0),

$$\begin{aligned} A_0(\lambda) &= \zeta_1^{(e)}(\lambda)\, e^{-2\gamma_0{}^{(e)} d_0} \left(B_0(\lambda) + E_s^+\right) \\ B_0(\lambda) &= e^{2\gamma_0{}^{(e)} d_{-1}} \frac{\zeta_1^{(e)}(\lambda) e^{-2\gamma_0{}^{(e)} d_0} E_s^+ + E_s^-}{1 - \zeta_1^{(e)}(\lambda)\zeta_{-1}^{(e)}(\lambda) e^{2\gamma_0{}^{(e)}(d_{-1} - d_0)}} \zeta_{-1}^{(e)}(\lambda) \\ C_0(\lambda) &= \zeta_1^{(m)}(\lambda)\, e^{-2\gamma_0{}^{(m)} d_0} \left(D_0(\lambda) + H_s^+\right) \\ D_0(\lambda) &= e^{2\gamma_0{}^{(m)} d_{-1}} \frac{\zeta_1^{(m)}(\lambda) e^{-2\gamma_0{}^{(m)} d_0} H_s^+ + H_s^-}{1 - \zeta_1^{(m)}(\lambda)\zeta_{-1}^{(m)}(\lambda) e^{2\gamma_0{}^{(m)}(d_{-1} - d_0)}} \zeta_{-1}^{(m)}(\lambda) \end{aligned} \tag{3.8}$$

For region (1),

$$
\begin{aligned}
A_1(\lambda) &= B_1(\lambda)\, Q^{TM} \\
B_1(\lambda) &= \frac{2\left(B_0(\lambda)+{E_s}^+\right)e^{-{\gamma_0}^{(e)}d_0}}{{\varepsilon_{1,0}}^+ e^{-{\gamma_1}^{(e)}d_0}+{\varepsilon_{1,0}}^- e^{-{\gamma_1}^{(e)}d_0}Q^{TM}} \\
C_1(\lambda) &= D_1(\lambda)\, Q^{TE} \\
D_1(\lambda) &= \frac{2\left(D_0(\lambda)+{H_s}^+\right)e^{-{\gamma_0}^{(m)}d_0}}{{\mu_{1,0}}^+ e^{-{\gamma_1}^{(m)}d_0}+{\mu_{1,0}}^- e^{-{\gamma_1}^{(m)}d_0}Q^{TE}}
\end{aligned}
\tag{3.9}
$$

As for physical reasons, $A_1 = C_1 = B_{-1} = D_{-1} = 0$, that confirms no reflection of the outward directed propagating wave at the boundary. Which leads to $Q^{TM} = Q^{TE} = R^{TM} = R^{TE} = 0$. So, four simultaneous equations are solved for TM waves with $B_1,\ A_0,\ B_0,\ A_{-1}$ as unknowns to be solved and for TE waves $D_1,\ C_0,\ D_0,\ C_{-1}$ as unknowns to be solved for three layered media. In our case of measuring magnetic fields from air we need $B_1,\ A_0,\ B_0$ and $D_1,\ C_0,\ D_0$.

Here,

$$
\begin{aligned}
\zeta_1^{(e)}(\lambda) &= \frac{\dot{\varepsilon}_{1,0}+e^{2{\gamma_1}^{(e)}d_0}Q^{TM}}{1+\dot{\varepsilon}_{1,0}e^{2{\gamma_1}^{(e)}d_0}Q^{TM}} = \dot{\varepsilon}_{1,0} = \frac{\varepsilon_{1,0}^-}{\varepsilon_{1,0}^+} = \frac{\frac{{\varepsilon'}_1}{{\varepsilon'}_0}-\frac{{\gamma_1}^{(e)}}{{\gamma_0}^{(e)}}}{\frac{{\varepsilon'}_1}{{\varepsilon'}_0}+\frac{{\gamma_1}^{(e)}}{{\gamma_0}^{(e)}}} \\
\zeta_{-1}^{(e)}(\lambda) &= \frac{\dot{\varepsilon}_{-1,0}+e^{-2{\gamma_{-1}}^{(e)}d_{-1}}R^{TM}}{1+\dot{\varepsilon}_{-1,0}e^{-2{\gamma_{-1}}^{(e)}d_{-1}}R^{TM}} = \dot{\varepsilon}_{-1,0} = \frac{\varepsilon_{-1,0}^-}{\varepsilon_{-1,0}^+} = \frac{\frac{{\varepsilon'}_{-1}}{{\varepsilon'}_0}-\frac{{\gamma_{-1}}^{(e)}}{{\gamma_0}^{(e)}}}{\frac{{\varepsilon'}_{-1}}{{\varepsilon'}_0}+\frac{{\gamma_{-1}}^{(e)}}{{\gamma_0}^{(e)}}} \\
\zeta_1^{(m)}(\lambda) &= \frac{\dot{\mu}_{1,0}+e^{2{\gamma_1}^{(m)}d_0}Q^{TE}}{1+\dot{\mu}_{1,0}e^{2{\gamma_1}^{(m)}d_0}Q^{TE}} = \dot{\mu}_{1,0} = \frac{\mu_{1,0^-}}{\mu_{1,0^+}} = \frac{\frac{\mu_1}{\mu_0}-\frac{{\gamma_1}^{(m)}}{{\gamma_0}^{(m)}}}{\frac{\mu_1}{\mu_0}+\frac{{\gamma_1}^{(m)}}{{\gamma_0}^{(m)}}} \\
\zeta_{-1}^{(m)}(\lambda) &= \frac{\dot{\mu}_{-1,0}+e^{-2{\gamma_{-1}}^{(m)}d_{-1}}R^{TE}}{1+\dot{\mu}_{-1,0}e^{-2{\gamma_{-1}}^{(m)}d_{-1}}R^{TE}} = \dot{\mu}_{-1,0} = \frac{\mu_{-1,0^-}}{\mu_{-1,0^+}} = \frac{\frac{\mu_{-1}}{\mu_0}-\frac{{\gamma_{-1}}^{(m)}}{{\gamma_0}^{(m)}}}{\frac{\mu_{-1}}{\mu_0}+\frac{{\gamma_{-1}}^{(m)}}{{\gamma_0}^{(m)}}}
\end{aligned}
\tag{3.10}
$$

For the elementary dipoles under consideration, source values derived by Kong in Ref. [27] are used. Numerical computation techniques of Eqs. (3.3) and (3.4) are described in below:

3.1.1 For Horizontal Magnetic Dipole

For horizontal magnetic dipole along x-direction (HMDx):

$$
\begin{aligned}
& n = 1 \\
& {S_1}^{TE}(\phi) = \cos\phi \\
& {S_1}^{TM}(\phi) = -\sin\phi \\
& H_s^{\pm} = \pm\left(-\tfrac{\tilde{m}\lambda^2}{8\pi}\right) \\
& E_s^{+} = E_s^{-} = \tfrac{i\tilde{m}\omega\mu_0\lambda^2}{8\pi\gamma_0^{(e)}}
\end{aligned}
\tag{3.11}
$$

So,

$$
\begin{aligned}
B_0(\lambda) &= e^{2\gamma_0{}^{(e)}d_{-1}}\frac{\zeta_1^{(e)}(\lambda)e^{-2\gamma_0{}^{(e)}d_0}E_s^+ + E_s^-}{1-\zeta_1^{(e)}(\lambda)\zeta_{-1}^{(e)}(\lambda)e^{2\gamma_0{}^{(e)}(d_{-1}-d_0)}}\zeta_{-1}^{(e)}(\lambda)\\
B_0(\lambda) &= e^{2\gamma_0{}^{(e)}d_{-1}}\frac{\zeta_1^{(e)}(\lambda)e^{-2\gamma_0{}^{(e)}d_0}\left(\frac{i\tilde{m}\omega\mu_0\lambda^2}{8\pi\gamma_0^{(e)}}\right)+\left(\frac{i\tilde{m}\omega\mu_0\lambda^2}{8\pi\gamma_0^{(e)}}\right)}{1-\zeta_1^{(e)}(\lambda)\zeta_{-1}^{(e)}(\lambda)e^{2\gamma_0{}^{(e)}(d_{-1}-d_0)}}\zeta_{-1}^{(e)}(\lambda)\\
\underline{\underline{B_0}}(\lambda) &= B_0(\lambda)/\lambda^2 = e^{2\sqrt{\lambda^2-k_0^2}d_{-1}}\frac{\zeta_1^{(e)}(\lambda)e^{-2\sqrt{\lambda^2-k_0^2}d_0}\left(\frac{i\tilde{m}\omega\mu_0}{8\pi\sqrt{\lambda^2-k_0^2}}\right)+\left(\frac{i\tilde{m}\omega\mu_0}{8\pi\sqrt{\lambda^2-k_0^2}}\right)}{1-\zeta_1^{(e)}(\lambda)\zeta_{-1}^{(e)}(\lambda)e^{2\sqrt{\lambda^2-k_0^2}(d_{-1}-d_0)}}\zeta_{-1}^{(e)}(\lambda)
\end{aligned}
$$

$$
\begin{aligned}
A_0(\lambda) &= \zeta_1^{(e)}(\lambda)e^{-2\gamma_0{}^{(e)}d_0}\left(B_0(\lambda)+E_s^+\right)\\
A_0(\lambda) &= \zeta_1^{(e)}(\lambda)e^{-2\sqrt{\lambda^2-k_0^2}d_0}\left(\lambda^2\underline{\underline{B_0}}(\lambda)+\frac{i\tilde{m}\omega\mu_0\lambda^2}{8\pi\sqrt{\lambda^2-k_0^2}}\right)\\
\underline{\underline{A_0}}(\lambda) &= A_0(\lambda)/\lambda^2 = \zeta_1^{(e)}(\lambda)e^{-2\sqrt{\lambda^2-k_0^2}d_0}\left(\underline{\underline{B_0}}(\lambda)+\frac{i\tilde{m}\omega\mu_0}{8\pi\sqrt{\lambda^2-k_0^2}}\right)
\end{aligned}
$$

$$
\begin{aligned}
D_0(\lambda) &= e^{2\gamma_0{}^{(m)}d_{-1}}\frac{\zeta_1^{(m)}(\lambda)e^{-2\gamma_0{}^{(m)}d_0}H_s^+ + H_s^-}{1-\zeta_1^{(m)}(\lambda)\zeta_{-1}^{(m)}(\lambda)e^{2\gamma_0{}^{(m)}(d_{-1}-d_0)}}\zeta_{-1}^{(m)}(\lambda)\\
D_0(\lambda) &= e^{2\gamma_0{}^{(m)}d_{-1}}\frac{\zeta_1^{(m)}(\lambda)e^{-2\gamma_0{}^{(m)}d_0}\left(-\frac{\tilde{m}\lambda^2}{8\pi}\right)+\left(\frac{\tilde{m}\lambda^2}{8\pi}\right)}{1-\zeta_1^{(m)}(\lambda)\zeta_{-1}^{(m)}(\lambda)e^{2\gamma_0{}^{(m)}(d_{-1}-d_0)}}\zeta_{-1}^{(m)}(\lambda)\\
\underline{\underline{D_0}}(\lambda) &= D_0(\lambda)/\lambda^2 = e^{2\sqrt{\lambda^2-k_0^2}d_{-1}}\frac{\zeta_1^{(m)}(\lambda)e^{-2\sqrt{\lambda^2-k_0^2}d_0}\left(-\frac{\tilde{m}}{8\pi}\right)+\left(\frac{\tilde{m}}{8\pi}\right)}{1-\zeta_1^{(m)}(\lambda)\zeta_{-1}^{(m)}(\lambda)e^{2\sqrt{\lambda^2-k_0^2}(d_{-1}-d_0)}}\zeta_{-1}^{(m)}(\lambda)
\end{aligned}
$$

$$
\begin{aligned}
C_0(\lambda) &= \zeta_1^{(m)}(\lambda)e^{-2\gamma_0{}^{(m)}d_0}\left(D_0(\lambda)+H_s^+\right)\\
C_0(\lambda) &= \zeta_1^{(m)}(\lambda)e^{-2\gamma_0{}^{(m)}d_0}\left(\lambda^2\underline{\underline{D_0}}(\lambda)-\frac{\tilde{m}\lambda^2}{8\pi}\right)\\
\underline{\underline{C_0}}(\lambda) &= C_0(\lambda)/\lambda^2 = \zeta_1^{(m)}(\lambda)e^{-2\sqrt{\lambda^2-k_0^2}d_0}\left(\underline{\underline{D_0}}(\lambda)-\frac{\tilde{m}}{8\pi}\right)
\end{aligned}
\tag{3.12}
$$

$$
\begin{aligned}
B_1(\lambda) &= \frac{2\left(B_0(\lambda)+{E_s}^+\right)e^{-2{\gamma_0}^{(e)}d_0}}{{\varepsilon_{1,0}}^+ e^{-2{\gamma_1}^{(e)}d_0}} \\
B_1(\lambda) &= \frac{2\left(\lambda^2\underline{\underline{B_0}}(\lambda)+\frac{i\tilde{m}\omega\mu_0\lambda^2}{8\pi\sqrt{\lambda^2-k_0^2}}\right)e^{-2{\gamma_0}^{(e)}d_0}}{{\varepsilon_{1,0}}^+ e^{-2{\gamma_1}^{(e)}d_0}} \\
\underline{\underline{B_1}}(\lambda) &= B_1(\lambda)/\lambda^2 = \frac{2\left(\underline{\underline{B_0}}(\lambda)+\frac{i\tilde{m}\omega\mu_0}{8\pi\sqrt{\lambda^2-k_0^2}}\right)e^{-2\sqrt{\lambda^2-k_0^2}d_0}}{{\varepsilon_{1,0}}^+ e^{-2\sqrt{\lambda^2-k_1^2}d_0}}
\end{aligned}
\tag{3.13}
$$

$$
\begin{aligned}
D_1(\lambda) &= \frac{2\left(D_0(\lambda)+{H_s}^+\right)e^{-2{\gamma_0}^{(m)}d_0}}{\mu_{1,0^+}e^{-2{\gamma_1}^{(m)}d_0}+\mu_{1,0^-}e^{-2{\gamma_1}^{(m)}d_0}Q_{TE}} \\
D_1(\lambda) &= \frac{2\left(\lambda^2\underline{\underline{D_0}}(\lambda)-\frac{\tilde{m}\lambda^2}{8\pi}\right)e^{-2{\gamma_0}^{(m)}d_0}}{\mu_{1,0^+}e^{-2{\gamma_1}^{(m)}d_0}} \\
\underline{\underline{D_1}}(\lambda) &= D_1(\lambda)/\lambda^2 = \frac{2\left(\underline{\underline{D_0}}(\lambda)-\frac{\tilde{m}}{8\pi}\right)e^{-2\sqrt{\lambda^2-k_0^2}d_0}}{\mu_{1,0^+}e^{-2\sqrt{\lambda^2-k_1^2}d_0}}
\end{aligned}
$$

From $\underline{\underline{A_0}}(\lambda)$, $\underline{\underline{B_0}}(\lambda)$ and $\underline{\underline{B_1}}(\lambda)$, it is clear that there are two branch cuts at $\lambda = \pm k_0$. As k_0 is complex in our case, we can avoid these points if we integrate Eqs. (3.3) and (3.4) along real line of integration path. Besides $H_1^{(1)}(r\lambda)$ is a singular function with singularity at $\lambda = 0$, which can be ignored by taking a small contour around the singular point. Figure 3.2 shows the integration path and according to which our integration should take the form as:

$$
\begin{aligned}
\int_{-\infty}^{+\infty}()\,d\lambda &= \left[\int_{-\infty}^{0^-}+\int_{c_\varepsilon}+\int_{0^+}^{+\infty}\right]()\,d\lambda \\
\int_{-\infty}^{+\infty}()\,d\lambda &= \left[\int_{-\infty}^{0^-}+\int_{0^+}^{+\infty}\right]()\,d\lambda+\int_{c_\varepsilon}()d\lambda \\
\int_{-\infty}^{+\infty}()\,d\lambda &= \mathrm{I}^1+\mathrm{I}^2
\end{aligned}
\tag{3.14}
$$

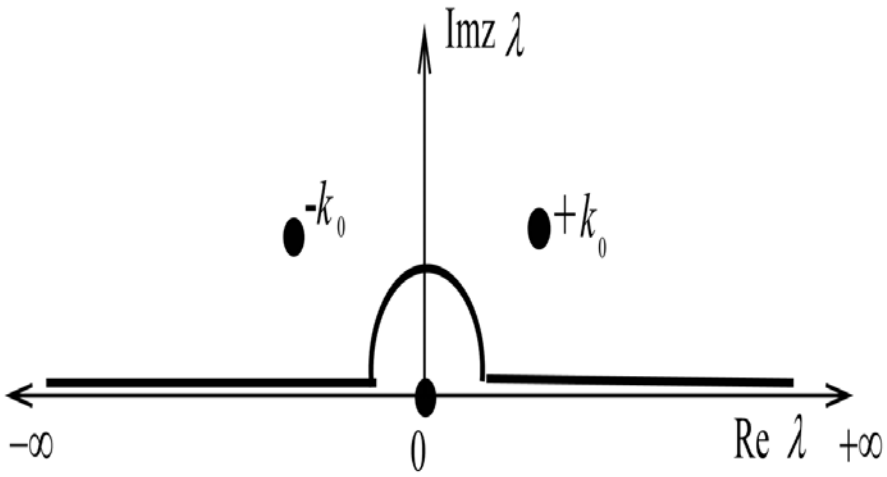

Figure 3.2: Integration Path

Along $\left[\int_{-\infty}^{0^-} + \int_{0^+}^{+\infty}\right]$, let $\lambda = \lambda_r$hence,$d\lambda = d\lambda_r$. So, ${\gamma_j}^{(e)} = \sqrt{{\lambda_r}^2 - k_j^2}$ and ${\gamma_j}^{(m)} = \sqrt{{\lambda_r}^2 - k_j^2}$.

Along $\int_{c_\varepsilon}$, let $\lambda = Re^{i\theta}$ hence $d\lambda = iRe^{i\theta}d\theta$, where $\pi \leq \theta \leq 0$.

So,

$$\begin{aligned} {\gamma_j}^{(e)} &= \lim_{R\to 0} \sqrt{(Re^{i\theta})^2 - k_j^2} \\ &= \lim_{R\to 0} ik_j \sqrt{1 - \left(\frac{Re^{i\theta}}{k_j}\right)^2} \\ &\approx \lim_{R\to 0} ik_j \left(1 - \tfrac{1}{2}\left(\frac{Re^{i\theta}}{k_j}\right)^2\right) \end{aligned} \tag{3.15}$$

After binomial expansion and taking the first two terms only, we can obtain the following expressions:

$$
\begin{aligned}
&\lim_{R\to 0} {\gamma_j}^{(e)} \approx ik_j \\
&\lim_{R\to 0} {\gamma_j}^{(m)} \approx ik_j \\
&\lim_{R\to 0} \zeta_1^{(e)}\left(Re^{i\theta}\right) \approx \zeta_1^{(e)} = \frac{\frac{{\varepsilon'}_1}{{\varepsilon'}_0} - \frac{{k_1}^{(e)}}{{k_0}^{(e)}}}{\frac{{\varepsilon'}_1}{{\varepsilon'}_0} + \frac{{k_1}^{(e)}}{{k_0}^{(e)}}} \\
&\lim_{R\to 0} \zeta_{-1}^{(e)}\left(Re^{i\theta}\right) \approx \zeta_{-1}^{(e)} = \frac{\frac{{\varepsilon'}_{-1}}{{\varepsilon'}_0} - \frac{{k_{-1}}^{(e)}}{{k_0}^{(e)}}}{\frac{{\varepsilon'}_{-1}}{{\varepsilon'}_0} + \frac{{k_{-1}}^{(e)}}{{k_0}^{(e)}}} \\
&\lim_{R\to 0} \zeta_1^{(m)}\left(Re^{i\theta}\right) \approx \zeta_1^{(m)} = \frac{\frac{\mu_1}{\mu_0} - \frac{ik_1}{ik_0}}{\frac{\mu_1}{\mu_0} + \frac{ik_1}{ik_0}} \\
&\lim_{R\to 0} \zeta_{-1}^{(m)}\left(Re^{i\theta}\right) \approx \zeta_{-1}^{(m)} = \frac{\frac{\mu_{-1}}{\mu_0} - \frac{ik_{-1}}{ik_0}}{\frac{\mu_{-1}}{\mu_0} + \frac{ik_{-1}}{ik_0}} \\
&\lim_{R\to 0} \underline{\underline{B_0}}\left(Re^{i\theta}\right) \approx \underline{\underline{B_0}} = e^{2ik_0 d_{-1}} \frac{\zeta_1^{(e)} e^{-2ik_0 d_0} 2\left(\frac{i\tilde{m}\omega\mu_0}{8\pi ik_0}\right)}{1-\zeta_1^{(e)}\zeta_{-1}^{(e)} e^{2ik_0(d_{-1}-d_0)}} \zeta_{-1}^{(e)} \\
&\lim_{R\to 0} \underline{\underline{B_1}}\left(Re^{i\theta}\right) \approx \underline{\underline{B_1}} = \frac{2\left(\underline{\underline{B_0}} + \frac{i\tilde{m}\omega\mu_0}{8\pi ik_0}\right) e^{-2ik_0 d_0}}{{\varepsilon_{1,0}}^{+} e^{-2ik_1 d_0}} \\
&\lim_{R\to 0} \underline{\underline{D_0}}\left(Re^{i\theta}\right) \approx \underline{\underline{D_0}} = e^{2ik_0 d_{-1}} \frac{\zeta_1^{(m)} e^{-2ik_0 d_0}\left(-\frac{\tilde{m}}{8\pi}\right) + \left(\frac{\tilde{m}}{8\pi}\right)}{1-\zeta_1^{(m)}\zeta_{-1}^{(m)} e^{2ik_0(d_{-1}-d_0)}} \zeta_{-1}^{(m)} \\
&\lim_{R\to 0} \underline{\underline{D_1}}\left(Re^{i\theta}\right) \approx \underline{\underline{D_1}} = \frac{2\left(\underline{\underline{D_0}} - \frac{\tilde{m}}{8\pi}\right) e^{-2ik_0 d_0}}{{\mu_{1,0}}^{+} e^{-2ik_1 d_0}} \\
&\lim_{R\to 0} H_1^{(1)}\left(rRe^{i\theta}\right) = \lim_{R\to 0} Re^{i\theta} H_1^{(1)}\left(rRe^{i\theta}\right) \\
&\approx \lim_{R\to 0} \left[\frac{-2i}{\pi r} + \left\{\frac{1}{2} + \frac{i\left(-1+2\Gamma-2\ln 2+2\ln\left(rRe^{i\theta}\right)\right)}{2\pi}\right\} r\left(Re^{i\theta}\right)^2 + O\left(r^3\left(Re^{i\theta}\right)^4\right)\right] \\
&= \frac{-2i}{\pi r}
\end{aligned}
\tag{3.16}
$$

Transverse Magnetic Mode

$$\begin{aligned}
\bar{H}_1^{TM}(r) &= \int_{-\infty}^{+\infty} d\lambda \left(\tfrac{-i\omega\varepsilon'_1}{\lambda^2 r} \alpha_1^+ (\lambda, z)\, H_1^{(1)}(r\lambda)\, S_1^{TM'}(\phi) \right) \\
&= \int_{-\infty}^{+\infty} \tfrac{-i\omega\varepsilon'_1}{\lambda^2 r} \left[A_1(\lambda)\, e^{\gamma_1^{(e)} z} + B_1(\lambda)\, e^{-\gamma_1^{(e)} z} \right] H_1^{(1)}(r\lambda)\, (-\cos\phi)\, d\lambda \\
&= \int_{-\infty}^{+\infty} \tfrac{i\omega\varepsilon'_1}{r} \left[\underline{\underline{A_1}}(\lambda)\, e^{\gamma_1^{(e)} z} + \underline{\underline{B_1}}(\lambda)\, e^{-\gamma_1^{(e)} z} \right] H_1^{(1)}(r\lambda)\, (\cos\phi)\, d\lambda
\end{aligned}$$

$$\mathrm{I}^1_{\bar{H}_1^{TM}(r)} = \left[\int_{-\infty}^{0^-} + \int_{0^+}^{+\infty} \right] \tfrac{i\omega\varepsilon'_1}{r} \left[\underline{\underline{A_1}}(\lambda_r)\, e^{\sqrt{{\lambda_r}^2 - k_1^2} z} + \underline{\underline{B_1}}(\lambda_r)\, e^{-\sqrt{{\lambda_r}^2 - k_1^2} z} \right] H_1^{(1)}(r\lambda_r)\, (\cos\phi)\, d\lambda_r$$

$$\begin{aligned}
\mathrm{I}^2_{\bar{H}_1^{TM}(r)} &= \lim_{R\to 0} \int_{\pi}^{0} \tfrac{i\omega\varepsilon'_1}{r} \left[\underline{\underline{A_1}}\left(Re^{i\theta}\right) e^{\gamma_1{}^{(e)} z} + \underline{\underline{B_1}}\left(Re^{i\theta}\right) e^{-\gamma_1{}^{(e)} z} \right] H_1^{(1)}\left(rRe^{i\theta}\right) (\cos\phi) \left(iRe^{i\theta} d\theta\right) \\
&= \lim_{R\to 0} \int_{\pi}^{0} \tfrac{-\omega\varepsilon'_1}{r} (\cos\phi) \left[\underline{\underline{A_1}}\left(Re^{i\theta}\right) e^{\gamma_1{}^{(e)} z} + \underline{\underline{B_1}}\left(Re^{i\theta}\right) e^{-\gamma_1{}^{(e)} z} \right] \left(Re^{i\theta} H_1^{(1)}\left(rRe^{i\theta}\right) \right) d\theta \\
&= \int_{\pi}^{0} \tfrac{-\omega\varepsilon'_1}{r} (\cos\phi) \left[\underline{\underline{A_1}} e^{ik_1 z} + \underline{\underline{B_1}} e^{-ik_1 z} \right] \times \tfrac{-2i}{\pi r} d\theta \\
&= \int_{\pi}^{0} \tfrac{i2\omega\varepsilon'_1}{\pi r^2} (\cos\phi) \left[\underline{\underline{A_1}} e^{ik_1 z} + \underline{\underline{B_1}} e^{-ik_1 z} \right] d\theta
\end{aligned} \tag{3.17}$$

$$\begin{aligned}
\bar{H}_1^{TM}(\phi) &= \int_{-\infty}^{+\infty} \tfrac{i\omega\varepsilon'_1}{\lambda} \left[A_1(\lambda) e^{\gamma_1^{(e)} z} + B_1(\lambda) e^{-\gamma_1^{(e)} z}\right] H_1^{(1)'}(r\lambda)(-\sin\phi) d\lambda \\
&= \int_{-\infty}^{+\infty} -\tfrac{i\omega\varepsilon'_1}{\lambda} \left[\lambda^2 \underline{\underline{A_1}}(\lambda) e^{\gamma_1^{(e)} z} + \lambda^2 \underline{\underline{B_1}}(\lambda) e^{-\gamma_1^{(e)} z}\right] \left(\tfrac{H_1^{(1)}(r\lambda)}{r\lambda} - H_2^{(1)}(r\lambda)\right) (\sin\phi) d\lambda \\
&= \int_{-\infty}^{+\infty} -i\omega\varepsilon'_1 \left[\underline{\underline{A_1}}(\lambda) e^{\gamma_1^{(e)} z} + \underline{\underline{B_1}}(\lambda) e^{-\gamma_1^{(e)} z}\right] \left(\tfrac{H_1^{(1)}(r\lambda)}{r} - \lambda H_2^{(1)}(r\lambda)\right) (\sin\phi) d\lambda
\end{aligned}$$

$$\begin{aligned}
\mathrm{I}^1_{\bar{H}_1^{TM}(\phi)} = &- \left[\int_{-\infty}^{0^-} + \int_{0^+}^{+\infty}\right] i\omega\varepsilon'_1 \left[\underline{\underline{A_1}}(\lambda_r) e^{\sqrt{{\lambda_r}^2 - k_1^2} z} + \underline{\underline{B_1}}(\lambda_r) e^{-\sqrt{{\lambda_r}^2 - k_1^2} z}\right] \\
&\left(\tfrac{H_1^{(1)}(r\lambda_r)}{r} - \lambda_r H_2^{(1)}(r\lambda_r)\right) (\sin\phi) d\lambda_r
\end{aligned}$$

$$\begin{aligned}
\mathrm{I}^2_{\bar{H}_1^{TM}(\phi)} = &\lim_{R\to 0} \int_{\pi}^{0} -i\omega\varepsilon'_1 \left[\underline{\underline{A_1}}\left(Re^{i\theta}\right) e^{{\gamma_1}^{(e)} z} + \underline{\underline{B_1}}\left(Re^{i\theta}\right) e^{-{\gamma_1}^{(e)} z}\right] \\
&\left(\tfrac{H_1^{(1)}\left(rRe^{i\theta}\right)}{r} - Re^{i\theta} H_2^{(1)}\left(rRe^{i\theta}\right)\right) (\sin\phi) \left(iRe^{i\theta} d\theta\right) \\
= &\lim_{R\to 0} \int_{\pi}^{0} \omega\varepsilon'_1 \left[\underline{\underline{A_1}}\left(Re^{i\theta}\right) e^{{\gamma_1}^{(e)} z} + \underline{\underline{B_1}}\left(Re^{i\theta}\right) e^{-{\gamma_1}^{(e)} z}\right] \\
&\left(\tfrac{\left(Re^{i\theta} H_1^{(1)}\left(rRe^{i\theta}\right)\right)}{r} - \left(Re^{i\theta}\right)^2 H_2^{(1)}\left(rRe^{i\theta}\right)\right) (\sin\phi) d\theta \\
= &\int_{\pi}^{0} \omega\varepsilon'_1 \left[\underline{\underline{A_1}} e^{ik_1 z} + \underline{\underline{B_1}} e^{-ik_1 z}\right] \times \tfrac{-2i}{\pi r^2} (\sin\phi) d\theta \\
= &\int_{\pi}^{0} \tfrac{-2i\omega\varepsilon'_1}{\pi r^2} (\sin\phi) \left[\underline{\underline{A_1}} e^{ik_1 z} + \underline{\underline{B_1}} e^{-ik_1 z}\right] d\theta
\end{aligned} \tag{3.18}$$

$$\overline{H}_1^{TM}(z) = 0 \tag{3.19}$$

Transverse Electric Mode

$$\begin{aligned}
\bar{H}_1^{TE}(r) &= \int_{-\infty}^{+\infty} d\lambda \left(\tfrac{-\gamma_1{}^{(m)}}{\lambda} \beta_1^-(\lambda, z)\ H_1^{(1)'}(r\lambda)\, S_1^{TE}(\phi) \right) \\
&= \int_{-\infty}^{+\infty} \tfrac{-\gamma_1{}^{(m)}}{\lambda} \left[-C_1(\lambda)\, e^{\gamma_1{}^{(m)} z} + D_1(\lambda)\, e^{-\gamma_1{}^{(m)} z} \right] \left(\tfrac{H_1^{(1)}(r\lambda)}{r\lambda} - H_2^{(1)}(r\lambda) \right) (\cos\phi)\, d\lambda \\
&= \int_{-\infty}^{+\infty} -\gamma_1{}^{(m)} \left[-\underline{\underline{C_1}}(\lambda)\, e^{\gamma_1{}^{(m)} z} + \underline{\underline{D_1}}(\lambda)\, e^{-\gamma_1{}^{(m)} z} \right] \left(\tfrac{H_1^{(1)}(r\lambda)}{r} - \lambda H_2^{(1)}(r\lambda) \right) (\cos\phi)\, d\lambda
\end{aligned}$$

$$\begin{aligned}
\therefore \mathrm{I}^1_{\bar{H}_1^{TE}(r)} = &- \left[\int_{-\infty}^{0^-} + \int_{0^+}^{+\infty} \right] \sqrt{{\lambda_r}^2 - k_1^2}\, (\cos\phi) \left[-\underline{\underline{C_1}}(\lambda_r)\, e^{\sqrt{{\lambda_r}^2 - k_1^2} z} + \underline{\underline{D_1}}(\lambda_r)\, e^{-\sqrt{{\lambda_r}^2 - k_1^2} z} \right] \\
&\left(\tfrac{H_1^{(1)}(r\lambda_r)}{r} - \lambda_r H_2^{(1)}(r\lambda_r) \right) d\lambda_r
\end{aligned}$$

$$\begin{aligned}
\mathrm{I}^2_{\bar{H}_1^{TE}(r)} = &\lim_{R\to 0} \int_{\pi}^{0} -\gamma_1{}^{(m)} \left[-\underline{\underline{C_1}}\left(Re^{i\theta}\right) e^{\gamma_1{}^{(m)} z} + \underline{\underline{D_1}}\left(Re^{i\theta}\right) e^{-\gamma_1{}^{(m)} z} \right] \\
&\left(\tfrac{H_1^{(1)}\left(rRe^{i\theta}\right)}{r} - Re^{i\theta} H_2^{(1)}\left(rRe^{i\theta}\right) \right) (\cos\phi) \left(iRe^{i\theta} d\theta \right) \\
= &\lim_{R\to 0} \int_{\pi}^{0} -i\gamma_1{}^{(m)} (\cos\phi) \left[-\underline{\underline{C_1}}\left(Re^{i\theta}\right) e^{\gamma_1{}^{(m)} z} + \underline{\underline{D_1}}\left(Re^{i\theta}\right) e^{-\gamma_1{}^{(m)} z} \right] \\
&\left(\tfrac{\left(Re^{i\theta} H_1^{(1)}\left(rRe^{i\theta}\right)\right)}{r} - \left(Re^{i\theta}\right)^2 H_2^{(1)}\left(rRe^{i\theta}\right) \right) d\theta \\
= &\int_{\pi}^{0} k_1 (\cos\phi) \left[-\underline{\underline{C_1}} e^{ik_1 z} + \underline{\underline{D_1}} e^{-ik_1 z} \right] \times \tfrac{-2i}{\pi r^2} d\theta \\
= &\int_{\pi}^{0} \tfrac{-2ik_1}{\pi r^2} (\cos\phi) \left[-\underline{\underline{C_1}} e^{ik_1 z} + \underline{\underline{D_1}} e^{-ik_1 z} \right] d\theta
\end{aligned} \tag{3.20}$$

$$\bar{H}_1^{TE}(\phi) = \int_{-\infty}^{+\infty} d\lambda \left(\frac{-\gamma_1{}^{(m)}}{\lambda^2 r} \beta_1^-(\lambda, z) H_1^{(1)}(r\lambda) S_1^{TE'}(\phi) \right)$$
$$= \int_{-\infty}^{+\infty} \frac{-\gamma_1{}^{(m)}}{\lambda^2 r} \left[-C_1(\lambda) e^{\gamma_1{}^{(m)} z} + D_1(\lambda) e^{-\gamma_1{}^{(m)} z} \right] H_1^{(1)}(r\lambda) (-\sin\phi) d\lambda$$
$$= \int_{-\infty}^{+\infty} \frac{\gamma_1{}^{(m)}}{r} \left[-\underline{\underline{C_1}}(\lambda) e^{\gamma_1{}^{(m)} z} + \underline{\underline{D_1}}(\lambda) e^{-\gamma_1{}^{(m)} z} \right] H_1^{(1)}(r\lambda) (\sin\phi) d\lambda$$

$$\therefore \mathrm{I}^1_{\bar{H}_1^{TE}(\phi)} = \left[\int_{-\infty}^{0^-} + \int_{0^+}^{+\infty} \right] \frac{\sqrt{\lambda_r{}^2 - k_1^2}}{r} (\sin\phi) \left[-\underline{\underline{C_1}}(\lambda_r) e^{\sqrt{\lambda_r{}^2 - k_1^2} z} + \underline{\underline{D_1}}(\lambda_r) e^{-\sqrt{\lambda_r{}^2 - k_1^2} z} \right] H_1^{(1)}(r\lambda_r) d\lambda_r$$

$$\mathrm{I}^2_{\bar{H}_1^{TE}(\phi)} = \lim_{R\to 0} \int_{\pi}^{0} \frac{\gamma_1{}^{(m)}}{r} \left[-\underline{\underline{C_1}}\left(Re^{i\theta}\right) e^{\gamma_1{}^{(m)} z} + \underline{\underline{D_1}}\left(Re^{i\theta}\right) e^{-\gamma_1{}^{(m)} z} \right] H_1^{(1)}\left(rRe^{i\theta}\right) (\sin\phi) \left(iRe^{i\theta} d\theta\right)$$
$$= \lim_{R\to 0} \int_{\pi}^{0} \frac{i\gamma_1{}^{(m)}}{r} (\sin\phi) \left[-\underline{\underline{C_1}}\left(Re^{i\theta}\right) e^{\gamma_1{}^{(m)} z} + \underline{\underline{D_1}}\left(Re^{i\theta}\right) e^{-\gamma_1{}^{(m)} z} \right] \left(Re^{i\theta} H_1^{(1)}\left(rRe^{i\theta}\right) \right) d\theta$$
$$= \int_{\pi}^{0} \frac{-k_1}{r} (\sin\phi) \left[-\underline{\underline{C_1}} e^{ik_1 z} + \underline{\underline{D_1}} e^{-ik_1 z} \right] \times \frac{-2i}{\pi r} d\theta$$
$$= \int_{\pi}^{0} \frac{2ik_1}{\pi r^2} (\sin\phi) \left[-\underline{\underline{C_1}} e^{ik_1 z} + \underline{\underline{D_1}} e^{-ik_1 z} \right] \times d\theta \tag{3.21}$$

$$\bar{H}_1^{TE}(z) = \int_{-\infty}^{+\infty} d\lambda \left(\beta_1^+(\lambda, z) \; H_1^{(1)}(r\lambda) S_1^{TE}(\phi) \right)$$
$$= \int_{-\infty}^{+\infty} \left[C_1(\lambda) e^{\gamma_1{}^{(m)} z} + D_1(\lambda) e^{-\gamma_1{}^{(m)} z} \right] H_1^{(1)}(r\lambda) (\cos\phi) d\lambda$$
$$= \int_{-\infty}^{+\infty} \left[\underline{\underline{C_1}}(\lambda) e^{\gamma_1{}^{(m)} z} + \underline{\underline{D_1}}(\lambda) e^{-\gamma_1{}^{(m)} z} \right] \lambda^2 H_1^{(1)}(r\lambda) (\cos\phi) d\lambda$$

$$\therefore \mathrm{I}^1_{\bar{H}_1^{TE}(z)} = \left[\int_{-\infty}^{0^-} + \int_{0^+}^{+\infty} \right] \lambda_r{}^2 \left[\underline{\underline{C_1}}(\lambda_r) e^{\sqrt{\lambda_r{}^2 - k_1^2} z} + \underline{\underline{D_1}}(\lambda_r) e^{-\sqrt{\lambda_r{}^2 - k_1^2} z} \right] H_1^{(1)}(r\lambda_r) (\cos\phi) d\lambda_r$$

$$\mathrm{I}^2_{\bar{H}_1^{TE}(z)} = \lim_{R\to 0} \int_{\pi}^{0} \left[\underline{\underline{C_1}}\left(Re^{i\theta}\right) e^{\gamma_1{}^{(m)} z} + \underline{\underline{D_1}}\left(Re^{i\theta}\right) e^{-\gamma_1{}^{(m)} z} \right] \left(Re^{i\theta}\right)^2 H_1^{(1)}\left(rRe^{i\theta}\right) (\cos\phi) \left(iRe^{i\theta} d\theta\right)$$
$$= \lim_{R\to 0} \int_{\pi}^{0} i\left(Re^{i\theta}\right)^2 (\cos\phi) \left[\underline{\underline{C_1}}\left(Re^{i\theta}\right) e^{\gamma_1{}^{(m)} z} + \underline{\underline{D_1}}\left(Re^{i\theta}\right) e^{-\gamma_1{}^{(m)} z} \right] \left(Re^{i\theta} H_1^{(1)}\left(rRe^{i\theta}\right) \right) d\theta$$
$$= 0 \tag{3.22}$$

Finally, for horizontal magnetic dipole

$$\tilde{\mathbf{H}}_1^{TM}\begin{bmatrix} r \\ \phi \\ z \end{bmatrix} = \begin{cases} \left[\int_{-\infty}^{0^-}+\int_{0^+}^{+\infty}\right]\frac{i\omega\varepsilon'_1}{r}\left[\underline{\underline{A_1}}\left(\lambda_r\right)e^{\sqrt{{\lambda_r}^2-k_1^2}z}+\underline{\underline{B_1}}\left(\lambda_r\right)e^{-\sqrt{{\lambda_r}^2-k_1^2}z}\right]H_1^{(1)}\left(r\lambda_r\right)\left(\cos\phi\right)d\lambda_r \\ \qquad +\int_{\pi}^{0}\frac{i2\omega\varepsilon'_1}{\pi r^2}\left(\cos\phi\right)\left[\underline{\underline{A_1}}e^{ik_1z}+\underline{\underline{B_1}}e^{-ik_1z}\right]d\theta \\ -\left[\int_{-\infty}^{0^-}+\int_{0^+}^{+\infty}\right]i\omega{\varepsilon'}_1\left(\sin\phi\right)\left[\underline{\underline{A_1}}\left(\lambda_r\right)e^{\sqrt{{\lambda_r}^2-k_1^2}z}+\underline{\underline{B_1}}\left(\lambda_r\right)e^{-\sqrt{{\lambda_r}^2-k_1^2}z}\right] \\ \left(\frac{H_1^{(1)}(r\lambda_r)}{r}-\lambda_r H_2^{(1)}\left(r\lambda_r\right)\right)d\lambda_r+\int_{\pi}^{0}\frac{-2i\omega\varepsilon'_1}{\pi r^2}\left(\sin\phi\right)\left[\underline{\underline{A_1}}e^{ik_1z}+\underline{\underline{B_1}}e^{-ik_1z}\right]d\theta \\ 0 \end{cases}$$

$$\tilde{\mathbf{H}}_1^{TE}\begin{bmatrix} r \\ \phi \\ z \end{bmatrix} = \begin{cases} -\left[\int_{-\infty}^{0^-}+\int_{0^+}^{+\infty}\right]\sqrt{{\lambda_r}^2-k_1^2}\left(\cos\phi\right)\left[-\underline{\underline{C_1}}\left(\lambda_r\right)e^{\sqrt{{\lambda_r}^2-k_1^2}z}+\underline{\underline{D_1}}\left(\lambda_r\right)e^{-\sqrt{{\lambda_r}^2-k_1^2}z}\right] \\ \left(\frac{H_1^{(1)}(r\lambda_r)}{r}-\lambda_r H_2^{(1)}\left(r\lambda_r\right)\right)d\lambda_r+\int_{\pi}^{0}\frac{-2ik_1}{\pi r^2}\left(\cos\phi\right)\left[-\underline{\underline{C_1}}e^{ik_1z}+\underline{\underline{D_1}}e^{-ik_1z}\right]d\theta \\ \left[\int_{-\infty}^{0^-}+\int_{0^+}^{+\infty}\right]\frac{\sqrt{{\lambda_r}^2-k_1^2}}{r}\left(\sin\phi\right)\left[-\underline{\underline{C_1}}\left(\lambda_r\right)e^{\sqrt{{\lambda_r}^2-k_1^2}z}+\underline{\underline{D_1}}\left(\lambda_r\right)e^{-\sqrt{{\lambda_r}^2-k_1^2}z}\right] \\ \qquad H_1^{(1)}\left(r\lambda_r\right)d\lambda_r+\int_{\pi}^{0}\frac{2ik_1}{\pi r^2}\left(\sin\phi\right)\left[-\underline{\underline{C_1}}e^{ik_1z}+\underline{\underline{D_1}}e^{-ik_1z}\right]\times d\theta \\ 0 \end{cases} \tag{3.23}$$

3.1.2 For Vertical Magnetic Dipole

$$\begin{aligned} & n=0 \\ & {S_o}^{TE}\left(\phi\right)=1 \\ & H_s^+=H_s^-=-\frac{\tilde{m}\lambda^3}{8\pi\gamma_0^{(m)}} \\ & E_s^+=E_s^-=0 \end{aligned} \tag{3.24}$$

So,

$$A = B = 0$$

$$\begin{aligned}
D_0(\lambda) &= e^{2\gamma_0{}^{(m)} d_{-1}} \frac{\zeta_1^{(m)}(\lambda) e^{-2\gamma_0{}^{(m)} d_0} H_s^+ + H_s^-}{1 - \zeta_1^{(m)}(\lambda)\zeta_{-1}^{(m)}(\lambda) e^{2\gamma_0{}^{(m)}(d_{-1}-d_0)}} \zeta_{-1}^{(m)}(\lambda) \\
D_0(\lambda) &= e^{2\gamma_0{}^{(m)} d_{-1}} \frac{\zeta_1^{(m)}(\lambda) e^{-2\gamma_0{}^{(m)} d_0} \left(-\frac{\tilde{m}\lambda^3}{8\pi\gamma_0^{(m)}}\right) + \left(-\frac{\tilde{m}\lambda^3}{8\pi\gamma_0^{(m)}}\right)}{1 - \zeta_1^{(m)}(\lambda)\zeta_{-1}^{(m)}(\lambda) e^{2\gamma_0{}^{(m)}(d_{-1}-d_0)}} \zeta_{-1}^{(m)}(\lambda) \\
\underline{\underline{D_0}}(\lambda) &= D_0(\lambda)/\lambda^3 = e^{2\sqrt{\lambda^2 - k_0^2} d_{-1}} \frac{\zeta_1^{(m)}(\lambda) e^{-2\sqrt{\lambda^2-k_0^2} d_0} \left(-\frac{\tilde{m}}{8\pi\sqrt{\lambda^2-k_0^2}}\right) + \left(-\frac{\tilde{m}}{8\pi\sqrt{\lambda^2-k_0^2}}\right)}{1 - \zeta_1^{(m)}(\lambda)\zeta_{-1}^{(m)}(\lambda) e^{2\sqrt{\lambda^2-k_0^2}(d_{-1}-d_0)}} \zeta_{-1}^{(m)}(\lambda)
\end{aligned}$$

$$\begin{aligned}
C_0(\lambda) &= \zeta_1^{(m)}(\lambda) e^{-2\gamma_0{}^{(m)} d_0} \left(D_0(\lambda) + H_s^+\right) \\
C_0(\lambda) &= \zeta_1^{(m)}(\lambda) e^{-2\gamma_0{}^{(m)} d_0} \left(\lambda^3 \underline{\underline{D_0}}(\lambda) - \frac{\tilde{m}\lambda^3}{8\pi\gamma_0^{(m)}}\right) \\
\underline{\underline{C_0}}(\lambda) &= C_0(\lambda)/\lambda^3 = \zeta_1^{(m)}(\lambda) e^{-2\sqrt{\lambda^2-k_0^2} d_0} \left(\underline{\underline{D_0}}(\lambda) - \frac{\tilde{m}}{8\pi\sqrt{\lambda^2-k_0^2}}\right)
\end{aligned} \tag{3.25}$$

$$\begin{aligned}
D_1(\lambda) &= \frac{2\left(D_0(\lambda) + H_s{}^+\right) e^{-2\gamma_0{}^{(m)} d_0}}{\mu_{1,0^+} e^{-2\gamma_1{}^{(m)} d_0} + \mu_{1,0^-} e^{-2\gamma_1{}^{(m)} d_0} Q_{TE}} \\
D_1(\lambda) &= \frac{2\left(\lambda^3 \underline{\underline{D_0}}(\lambda) - \frac{\tilde{m}\lambda^3}{8\pi\gamma_0^{(m)}}\right) e^{-2\gamma_0{}^{(m)} d_0}}{\mu_{1,0^+} e^{-2\gamma_1{}^{(m)} d_0}} \\
\underline{\underline{D_1}}(\lambda) &= D_1(\lambda)/\lambda^3 = \frac{2\left(\underline{\underline{D_0}}(\lambda) - \frac{\tilde{m}}{8\pi\sqrt{\lambda^2-k_0^2}}\right) e^{-2\sqrt{\lambda^2-k_0^2} d_0}}{\mu_{1,0^+} e^{-2\sqrt{\lambda^2-k_1^2} d_0}}
\end{aligned} \tag{3.26}$$

Following the similar integration procedure of Fig. 3.2 developed in Section 3.1.1 for horizontal magnetic dipole we can obtain the expressions for vertical magnetic dipole also.

Transverse Magnetic Mode

As $A = B = 0$, for vertical magnetic dipole source:

$$\tilde{\mathbf{H}}_1^{TM}(r,\phi,z) = \begin{cases} 0 \\ 0 \\ 0 \end{cases} \tag{3.27}$$

Transverse Electric Mode

$$\begin{aligned}
\bar{H}_1^{TE}(r) &= \int_{-\infty}^{+\infty} d\lambda \left(\tfrac{-\gamma_1{}^{(m)}}{\lambda} \left(\beta_1^-(\lambda,z)\ H_0^{(1)'}(r\lambda)\, S_0^{TE}(\phi) \right) \right) \\
&= \int_{-\infty}^{+\infty} \tfrac{-\gamma_1{}^{(m)}}{\lambda} \left[-C_1(\lambda)\, e^{\gamma_1{}^{(m)}z} + D_1(\lambda)\, e^{-\gamma_1{}^{(m)}z} \right] \left(\tfrac{0 \times H_0^{(1)}(r\lambda)}{r\lambda} - H_1^{(1)}(r\lambda) \right) d\lambda \\
&= \int_{-\infty}^{+\infty} \lambda^2 \gamma_1{}^{(m)} \left[-\underline{\underline{C_1}}(\lambda)\, e^{\gamma_1{}^{(m)}z} + \underline{\underline{D_1}}(\lambda)\, e^{-\gamma_1{}^{(m)}z} \right] H_1^{(1)}(r\lambda) d\lambda
\end{aligned}$$

$$\therefore \mathrm{I}^1_{\bar{H}_1^{TE}(r)} = \left[\int_{-\infty}^{0^-} + \int_{0^+}^{+\infty} \right] {\lambda_r}^2 \sqrt{\lambda^2 - k_1^2} \left[-\underline{\underline{C_1}}(\lambda_r)\, e^{\sqrt{\lambda^2-k_1^2}z} + \underline{\underline{D_1}}(\lambda_r)\, e^{-\sqrt{\lambda^2-k_1^2}z} \right] H_1^{(1)}(r\lambda_r)\, d\lambda_r$$

$$\begin{aligned}
\mathrm{I}^2_{\bar{H}_1^{TE}(r)} &= \lim_{R\to 0} \int_{\pi}^{0} \left(Re^{i\theta}\right)^2 \gamma_1{}^{(m)} \left[-\underline{\underline{C_1}}\left(Re^{i\theta}\right) e^{\gamma_1{}^{(m)}z} + \underline{\underline{D_1}}\left(Re^{i\theta}\right) e^{-\gamma_1{}^{(m)}z} \right] H_1^{(1)}\left(rRe^{i\theta}\right) \left(iRe^{i\theta} d\theta\right) \\
&= 0
\end{aligned} \tag{3.28}$$

$$\begin{aligned}
\bar{H}_1^{TE}(\phi) &= \int_{-\infty}^{+\infty} d\lambda \left(\tfrac{-\gamma_1{}^{(m)}}{\lambda^2 r} \beta_1^-(\lambda,z)\ H_0^{(1)}(r\lambda)\, S_0^{TE'}(\phi) \right) \\
&= 0
\end{aligned} \tag{3.29}$$

$$\bar{H}_1^{TE}(z) = \int_{-\infty}^{+\infty} d\lambda \left(\beta_1^+(\lambda, z)\ H_0^{(1)}(r\lambda)\, S_0^{TE}(\phi)\right)$$
$$= \int_{-\infty}^{+\infty} \left[C_1(\lambda)\, e^{\gamma_1{}^{(m)} z} + D_1(\lambda)\, e^{-\gamma_1{}^{(m)} z}\right] H_0^{(1)}(r\lambda) d\lambda$$
$$= \int_{-\infty}^{+\infty} \lambda^3 \left[\underline{\underline{C_1}}(\lambda)\, e^{\gamma_1{}^{(m)} z} + \underline{\underline{D_1}}(\lambda)\, e^{-\gamma_1{}^{(m)} z}\right] H_0^{(1)}(r\lambda) d\lambda$$

$$\therefore \mathrm{I}^1_{\bar{H}_1^{TE}(z)} = \left[\int_{-\infty}^{0^-} + \int_{0^+}^{+\infty}\right] {\lambda_r}^3 \left[\underline{\underline{C_1}}(\lambda_r)\, e^{\sqrt{\lambda^2 - k_1^2} z} + \underline{\underline{D_1}}(\lambda_r)\, e^{-\sqrt{\lambda^2 - k_1^2} z}\right] H_0^{(1)}(r\lambda_r)\, d\lambda_r$$

$$\mathrm{I}^2_{\bar{H}_1^{TE}(z)} = \lim_{R\to 0} \int_{\pi}^{0} \left(Re^{i\theta}\right)^3 \left[\underline{\underline{C_1}}\left(Re^{i\theta}\right) e^{\gamma_1{}^{(m)} z} + \underline{\underline{D_1}}\left(Re^{i\theta}\right) e^{-\gamma_1{}^{(m)} z}\right] H_0^{(1)}\left(rRe^{i\theta}\right)\left(iRe^{i\theta} d\theta\right)$$
$$= 0 \tag{3.30}$$

Finally, for vertical magnetic dipole,

$$\tilde{\mathbf{H}}_1^{TM} \begin{bmatrix} r \\ \phi \\ z \end{bmatrix} = \begin{cases} 0 \\ 0 \\ 0 \end{cases}$$

$$\tilde{\mathbf{H}}_1^{TE} \begin{bmatrix} r \\ \phi \\ z \end{bmatrix} = \begin{cases} \left[\int_{-\infty}^{0^-} + \int_{0^+}^{+\infty}\right] {\lambda_r}^2 \sqrt{\lambda^2 - k_1^2} \left[-\underline{\underline{C_1}}(\lambda_r)\, e^{\sqrt{\lambda^2 - k_1^2} z} + \underline{\underline{D_1}}(\lambda_r)\, e^{-\sqrt{\lambda^2 - k_1^2} z}\right] \\ \qquad\qquad H_1^{(1)}(r\lambda_r)\, d\lambda_r \\ 0 \\ \left[\int_{-\infty}^{0^-} + \int_{0^+}^{+\infty}\right] {\lambda_r}^3 \left[\underline{\underline{C_1}}(\lambda_r)\, e^{\sqrt{\lambda^2 - k_1^2} z} + \underline{\underline{D_1}}(\lambda_r)\, e^{-\sqrt{\lambda^2 - k_1^2} z}\right] H_0^{(1)}(r\lambda_r)\, d\lambda_r \end{cases} \tag{3.31}$$

These final equations are solved numerically using Legendre-Gauss Quadrature Weights and Nodes [28]. The integrands in each of the cases have significant values

within $[-3, 3]$, and 5000 points are used to evaluate nodes and weights within this limit.

3.2 MODELING MAGNETIZATION OF TARGET

The main source of the static magnetic field of a target is the ferromagnetic material (used for its fabrication), which is magnetized due to its external magnetic field. The instantaneous magnetization of a body depends not only on the presence of a magnetic field, but also on the history of the field. Additionally, stress and ambient temperature influence magnetization. The complicated interrelationship between the magnetic field, history, stress and magnetization can be demonstrated by magneto-mechanical models. When a ship or submarine hull is being fabricated, it is subjected to heat (welding) and to impact (riveting). Ferrous metal contains groups of iron molecules called "domains." Each domain is a tiny magnet, and has its own magnetic field with a north and south pole. When the domains are not aligned along any axis, but point in different directions at random, there is a negligible magnetic pattern. However, if the metal is put into a constant magnetic field and its particles are agitated, as they would be by hammering or by heating, the domains tend to orient themselves so that their north poles point toward the south pole of the field, and their south poles point toward the north pole of the field. All the fields of the domains then have an additive effect, and a piece of ferrous metal so treated has a magnetic field of its own. Although the earth's magnetic field is not strong, a ship's hull contains so much steel that it acquires a significant and permanent magnetic field during construction. The steel in a ship also has the effect of causing

earth's lines of force (flux) to move out of their normal positions and be concentrated at the ship. This is called the "induced field," and varies with the heading of the ship. A magnetized body also produces a secondary magnetic field that can be measured externally. This field is a major contributor to its magnetic signature. Given the distribution of a targets magnetization, its signature can be calculated which is expressed in static magnetic dipole (DC Dipole). Since the distribution of earths magnetic field over the oceans has been mapped extensively and modeled, magnetostatics models can be used to predict a targets magnetic signature as a function of its position and heading [29]. An example of a modeled DC Dipole-like magnetic signature of a submarine for a given target depth is shown in Fig. 3.3.

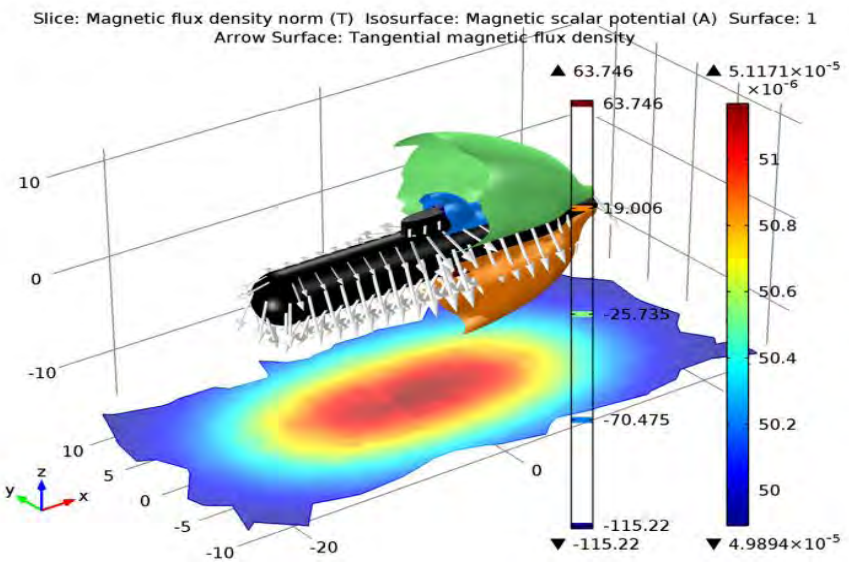

Figure 3.3: Magnetic Signature of a Submarine (Submarine: Image courtesy of Kockums AB.)

Additionally, when an electrically conductive object moves through the earths magnetic field, it generates an ELF magnetic field that can be externally measured. Thus, the target signal contains both a DC Dipole-like signal (due to the

magnetization of the target) and an ELF magnetic field (induced by its motion through the earths magnetic field).

The static magnetization of a ferromagnetic body due to it's external earth's magnetic field can be calculated by

$$\vec{m} = \sum\nolimits_{i=1}^{N_d} \overrightarrow{\mathrm{M}}_i = \sum\nolimits_{i=1}^{N_d} \chi_v \overrightarrow{\mathrm{H}}_i \left|\Delta \vec{V}_i\right| \tag{3.32}$$

Where, the whole target is divided into N_d number of small volumetric elements.

small volume element,

$$\Delta \vec{V}_i = \Delta \vec{A}_i * t_d = \left\{(\vec{p}_1 - \vec{p}_0) \times (\vec{p}_2 - \vec{p}_0)\right\}_i * t_d$$

Here, volume magnetic susceptibility of the material, $\chi_v = \mu_r - 1$, magnetic moment due to $\Delta \vec{V}_i$ is $\vec{\mathrm{M}}_i$, total magnetization of the ship is $\vec{m}$, two adjacent sides of any rectangle are $(\vec{p}_1 - \vec{p}_0)$ and $(\vec{p}_2 - \vec{p}_0)$, small area element is $\Delta \vec{A}_i$, thickness of the steel is t_d, external earth's magnetic field intensity at i^{th} element is $\overrightarrow{\mathrm{H}}_i$.

The resulted equivalent magnetic moment from Eq. (3.32) will be used as a dipole sources, $\tilde{m}\,(= I\mathrm{A})$ in Eqs. (3.2) using the computation techniques developed in Secs. 3.1.1 and 3.1.2 to generate target signature. So, target signal is

$$\mathbf{B}_{target}\,(x, y, z, t) = \mu_1 \tilde{\mathbf{H}}_{target}\,(x, y, z)\, e^{-i(w_{target} t + \psi_{target})} \tag{3.33}$$

Here, ψ_{target} is the initial phase of the target.

3.3 MODELING SOURCES OF NOISE

To consider the effect of distributed noise in the ocean environment, the noise sources can be modeled as small electric and magnetic dipoles which generate low

frequency electromagnetic induced noise signals. Equations (3.3) and (3.4) are developed for calculating magnetic field intensity due to a single dipole embedded in a stratified media. But for noise modelling, concept of multiple dipole sources come into consideration, and global coordinate system is developed. A geometrical representation is presented to illustrate the hypothetical concept of multiple sources in Fig. 3.4.

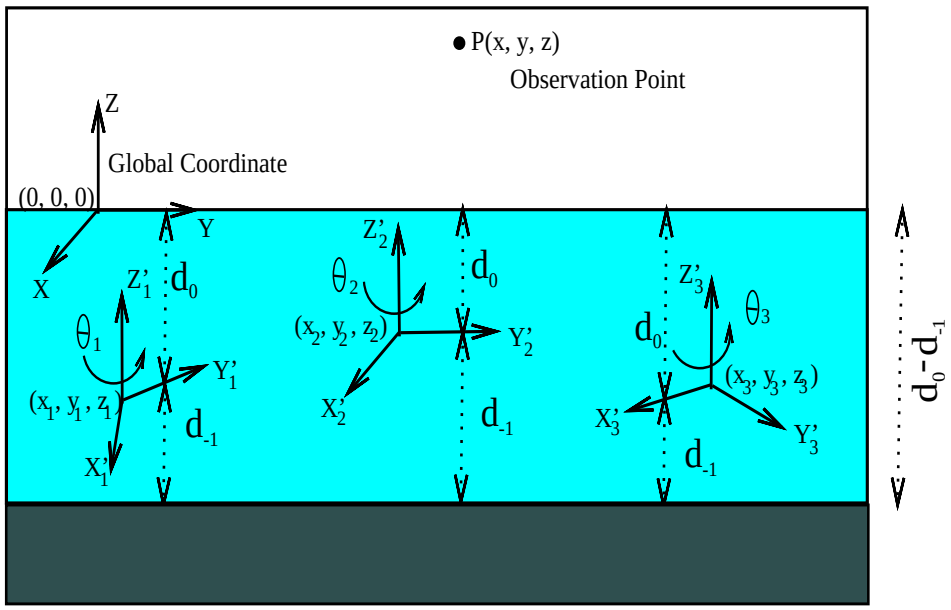

Figure 3.4: Geometric Representation of Multiple Dipole Sources Placement

Dipoles are placed at position (x_l, y_l, z_l) with their orientation θ_l and initial phases ψ_l, where l identifies dipole number. Global coordinate is at air-water interface and each dipole is considered to be in the origin of respective local coordinates to match the equations developed in Sec. 3.1 for single dipole. For convenience all the values are converted into Cartesian coordinate system. So a transformation matrix governing the translation and rotation can be used in order

to map the global coordinates to local frame of references, so that identical equations can be used to determine the field values. Therefore time-varying noise signal can be obtained by:

$$\mathbf{B}_{noise}(x,y,z,t) = \sum_{l=1}^{N_m} \mu_j \tilde{\mathbf{H}}_j\left(x'_l, y'_l, z'_l\right) e^{-i(\omega_l t+\psi_l)} \tag{3.34}$$

Here N_m is the total number of dipoles and $\mathrm{Re}\{\}$ represents real value of the argument. The position of observation point with reference to local coordinate system is obtained for individual dipoles using the following transformation:

$$\begin{bmatrix} x'_l \\ y'_l \\ z'_l \end{bmatrix} = \left[R_{z'}(\theta_l)\right]^{-1} \begin{bmatrix} x - x_l \\ y - y_l \\ z - z_l \end{bmatrix} \tag{3.35}$$

Where, the rotation matrix with respect to z' axis is

$$R_{z'}(\theta_l) = \begin{bmatrix} \cos\theta_l & -\sin\theta_l & 0 \\ \sin\theta_l & \cos\theta_l & 0 \\ 0 & 0 & 1 \end{bmatrix}$$

It is noted that prime coordinates refer to positions with respect to local frame of reference.

3.4 SIGNAL RECEIVED BY MAD SENSOR

The noisy magnetic signal observed by MAD sensor is composed of unwanted noise signal and desired target signal. So, the noisy magnetic signal is,

$$\mathbf{B}_{noisy}(x,y,z,t) = \mathbf{B}_{\text{target}}(x,y,z,t) + \mathbf{B}_{noise}(x,y,z,t) \tag{3.36}$$

This signal will be the observed/measured signal for detection, classification, localisation and tracking system.

Chapter 4

PROPOSED DETECTION, CLASSIFICATION, LOCALISATION AND TRACKING SYSTEM

The type of surveillance system used is highly dependent on the type of operation or mission, and that in many cases different systems can be combined to yield increased performance. The most important considerations are the size of the region of interest and the desired accuracy. In this chapter we describe the proposed method and mathematical foundation of the determination of the target, and estimation of the magnetic moment and motion parameters of the body from the magnetic signature.

4.1 DETECTION METHOD

EMD is a noise reduction algorithm which is intuitive and adaptive, with basic functions derived fully from the data. Compared to other denoising methods such as; filtering, independent and principle component analysis, neural networks, and

adaptive filtering, EMD is found more effective in the reduction of noise from the MAD signals. The computation of EMD does not require any previously known value of the signal. The key task here is to identify the intrinsic oscillatory modes by their characteristic time scales in the signal empirically, and accordingly, decompose the signal into intrinsic mode functions (IMFs). As a result, EMD is especially applicable for nonlinear and non-stationary signals, such as MAD signals.

A function is considered to be an IMF if it satisfies two conditions; First, In the whole data set, the number of local extrema and that of zero crossings must be equal to each other or different by at most one and second, at any point, the mean value of the envelope defined by the local maxima and that defined by the local minima should be zero. The systematic way to decompose the data into IMFs, known as the "sifting" process, is described as follows,

- All the local maxima of the data $\mathbf{B}_{noisy}[n]$ are determined and joined by cubic spline line as the upper envelope.

- All the local minima of the data $\mathbf{B}_{noisy}[n]$ are found and connected by cubic spline line as the lower envelope.

- In the first sifting process, the mean m_1 of the upper and lower envelops is first determined, and then, subtracted from the original data $\mathbf{B}_{noisy}[n]$ to obtain the first component $h_1[n]$ as,

$$h_1[n] = \mathbf{B}_{noisy}[n] - m_1 \tag{4.1}$$

  If $h_1[n]$ satisfies the conditions to be an IMF as mentioned above, it is considered as the first IMF $c_1[n]$.

- If $h_1[n]$ dissatisfies the conditions to be an IMF, it is treated as the data in the second sifting process, where steps 1, 2 and 3 are repeated on $h_1[n]$ to derive the second component $h_2[n]$ as,

$$h_2[n] = h_1[n] - m_2 \tag{4.2}$$

where, m_2 is the mean value determined from $h_1[n]$ with a view to determine $c_1[n]$ from $h_2[n]$, the conditions to be satisfied to be an IMF is checked for $h_2[n]$. If $h_2[n]$ does not satisfy the conditions, a standard difference (SD) is calculated from the two consecutive sifting results, namely $h_{i-1}[n]$ and $h_i[n]$ as

$$SD = \sum_{n=0}^{N} \frac{|h_{i-1}[n] - h_i[n]|^2}{h_{i-1}^2[n]} \tag{4.3}$$

When the value of SD resides within a predefined range, the sifting process is terminated, and $h_i[n]$ is termed as $c_1[n]$.

- once $c_1[n]$ is obtained, it is then subtracted from the original data to get a residue $r_1[n]$,

$$r_1[n] = \mathbf{B}_{noisy}[n] - c_1[n] \tag{4.4}$$

The residue $r_1[n]$ is treated as a new signal, and sifting process as described above is carried out on $r_1[n]$ to obtain the next residue signal $r_2[n]$. Therefore, the residue signal thus obtained can be expressed in general as,

$$r_j[n] = r_{j-1}[n] - c_j[n] \tag{4.5}$$

If $r_1[n]$ becomes a constant or monotonic function, the process of decomposing the signal into IMFs is terminated. So, the stopping criterion is,

$$\begin{aligned} A_{mean} &= abs\left(\Lambda_{\max} + \Lambda_{\min}\right)/2 \\ A_{env} &= abs\left(\Lambda_{\max} - \Lambda_{\min}\right)/2 \\ \tfrac{A_{mean}}{A_{env}} &< \tau_2 \\ \tfrac{A_{mean}}{A_{env} > \tau} &< tol \end{aligned} \tag{4.6}$$

To this end, for a L level decomposition, the original signal x[n] can be represented as the sum of the decomposed IMFs and resulting residue $r_L[n]$ as given by,

$$\mathbf{B}_{noisy}[n] = \sum_{i=1}^{L-1} c_i[n] + r_L[n] \tag{4.7}$$

4.2 CLASSIFICATION, LOCALISATION AND TRACKING METHOD

After the detection, the monitoring of ocean activities requires the localisation, classification and trajectory of enemy targets. Sometimes classification is known, only current status of the target (Position and velocity) are necessary like for ROV, AUV. So, the state parameters are magnetic moment, position and velocity of the target. These state parameters which change over time need to be determined using a sequence of noisy measurements (observations) made on the UAV based MAD system.

4.2.1 Dynamic state-space model

We wish to estimate the states of a non-linear dynamic system of the form:

$$\mathbf{x}_{k+1} = \mathbf{f}\left(\mathbf{x}_k, \mathbf{u}_k, \mathbf{v}_k\right) \tag{4.8}$$

$$\mathbf{B}_{noisy_k} = \mathbf{h}\left(\mathbf{x}_k, \mathbf{u}_k\right) + \mathbf{w}_k \tag{4.9}$$

Equation (4.8) represents the process model, while Eq. (4.9) represents the measurement (observation) model. Here, $\mathbf{x}_k$ is the n_x-dimensional state vector of the system at time step k, $\mathbf{u}_k$ is the input vector, $\mathbf{B}_{noisy_k}$ is the n_z-dimensional observation vector, and $\mathbf{v}_k$ and $\mathbf{w}_k$ are vectors representing the process and measurement noise, with dimensions n_v and n_w respectively. It is assumed that the noise vectors are independent of current and past states, and identically distributed.

First, the filter updates the state of the system given a state estimate $\hat{\mathbf{x}}_{k|k}$. The covariance of this estimate is $\mathbf{P}_{k+1|k}$.

$$x_{k+1|k} = E\left[\mathbf{f}\left[\mathbf{x}_k, \mathbf{u}_k, \mathbf{v}_k\right]|\mathbf{B}_{noisy_k}\right] \tag{4.10}$$

$$\mathbf{P}_{k+1|k} = E\left[\left(\mathbf{x}_{k+1} - \hat{\mathbf{x}}_{k+1|k}\right)\left(\mathbf{x}_{k+1} - \hat{\mathbf{x}}_{k+1|k}\right)^T|\mathbf{B}_{noisy_k}\right] \tag{4.11}$$

The problem of tracking a magnetic dipole does not satisfy the original Kalman filter requirements because the system observation $\mathbf{h}\left(\bullet\right)$ is non-linear. In order to deal with non-linear systems, two categories of techniques have been developed: parametric and non-parametric. The parametric techniques are based on improvements in linearizing the equations of the Kalman filter that is Unscented Kalman filter (UKF) and the non-parametric techniques are based on Monte Carlo simulations that is Particle Filter (PF).

4.2.2 Magnetic dipole dynamics and measurements

The target is fully characterised by its motion parameters (position and velocity) and the value of the magnetic dipole moment. When all these parameters are known the target may be classified as a certain mass or length, which can be appreciated after the amount of ferromagnetic material contained. Ship motion is rather slow and could be described using a constant velocity model. This mathematical model is sufficient to provide satisfactory estimation accuracy under the condition that the target does not accelerate during the observation time. During this period it is less probable that the target undergoes abrupt maneuvers. Also the magnetic mass of the target remains constant during the passage and can be estimated from the values of the equivalent magnetic dipole moment.

Let consider that the time increment between the data samples is Δt in sec, m is the magnetic moment of the dipole, $V\ [V_X,\ V_Y,\ V_Z = 0]$ is the velocity vector in m/sec, and $r\ [r_X,\ r_Y,\ r_Z]$ is the position vector from the global coordinate to the dipole in m. For a full characterization of the target, the entire system at time step k can be represented by the state vector:

$$\mathbf{x}_k = (r_X,\ r_Y,\ r_Z,\ V_X,\ V_Y,\ m)^T \tag{4.12}$$

The discrete equations of target motion are obtained using the piece-wise

approximation:

$$\begin{aligned} r_X(k) &= r_X(k-1) + \Delta t\, V_X \\ r_Y(k) &= r_Y(k-1) + \Delta t\, V_Y \\ r_Z(k) &= r_Z(k-1) \\ \\ V_X(k) &= V_X(k-1) \\ V_Y(k) &= V_Y(k-1) \\ \\ m(k) &= m(k-1) \end{aligned} \tag{4.13}$$

These are the process equations. Tri-axial magnetic sensors measure the observation data $\mathbf{B}_{noisy}$ at a given point due to a magnetic dipole by measurement equations developed in Chapter 3. So, the process function $\mathbf{f}(\bullet)$ in Eq. (4.8) is linear, but the measurement function $\mathbf{h}(\bullet)$ in Eq. (4.9) is highly non-linear. For one sensor, the measurement vector at time k has the form:

$$B_{noisy_k} = (B_x,\ B_y,\ B_z)^T \tag{4.14}$$

4.2.3 State Vector Estimation

Unscented Kalman Filter

The Kalman filter assumes a linear relationship for both system dynamics and observation equations, and a Gaussian distribution of the state vector. A Gaussian distribution can be represented by a mean and a covariance matrix. The Kalman filter propagates the first two moments of the distribution of the state vector recursively and has a distinctive predictor-corrector structure. The advantage of

a UKF over a traditional Extended Kalman Filter (EKF) is that the UKF can be more accurate when the propagation/measurement functions are not zero-mean w.r.t., the error (that is, they are significantly nonlinear in terms of their errors). Further, since a UKF doesn't require Jacobians, it's often easier to use a UKF than an EKF. By linearizing the non-linear function around the predicted state values, UKF can be used to solve the highly non-linear magnetic dipole tracking problem. UKF represents a method to calculate the first two moments (mean and covariance) of a random variable following the unscented transformation. These estimates of the mean and covariance are accurate to the second order of the Taylor series expansion. Errors are introduced in the third and higher order moments, but are scaled by the choice of a scaling parameter.

Particle Filter

Particle filter (PF) or Sequential Monte Carlo (SMC) methodology uses a genetic type mutation-selection sampling approach, with a set of particles (also called individuals, or samples) to represent the posterior distribution of some stochastic process given some noisy and/or partial observations. The state-space model can be non-linear, and the initial state and noise distributions can take any form required. Each particle has a likelihood weight assigned to it that represents the probability of that particle being sampled from the probability density function. Weight disparity leading to weight collapse is a common issue encountered in these filtering algorithms; however it can be mitigated by including a resampling step before the weights become too uneven.

From the Bayesian perspective, it is required to estimate $p\left(\mathbf{x}_k|\mathbf{B}_{noisy_{1:k}}\right)$ assuming that the pdf at time (k-1), $p\left(\mathbf{x}_{k-1}|\mathbf{B}_{noisy_{1:k-1}}\right)$ is available. The first

step in this process is called prediction and makes use of equation (4.8), which is assumed to describe a Markov process of order one:

$$p\left(\mathbf{x}_k|\mathbf{B}_{noisy_{1:k-1}}\right) = \int p\left(\mathbf{x}_k|\mathbf{x}_{k-1}\right)p\left(\mathbf{x}_{k-1}|\mathbf{B}_{noisy_{1:k-1}}\right)d\mathbf{x}_{k-1} \tag{4.15}$$

The second step, the measurement update, uses the most recent observation to produce the desired pdf via Bayes rule:

$$\begin{aligned} p\left(\mathbf{x}_k|\mathbf{B}_{noisy_{1:k}}\right) &= \frac{p\left(\mathbf{B}_{noisy_k}|\mathbf{x}_k\right)p\left(\mathbf{x}_k|\mathbf{B}_{noisy_{1:k-1}}\right)}{p\left(\mathbf{B}_{noisy_k}|\mathbf{B}_{noisy_{1:k-1}}\right)} \\ p\left(\mathbf{B}_{noisy_k}|\mathbf{B}_{noisy_{1:k-1}}\right) &= \int p\left(\mathbf{B}_{noisy_k}|\mathbf{x}_k\right)p\left(\mathbf{x}_k|\mathbf{B}_{noisy_{1:k-1}}\right)d\mathbf{x}_k \end{aligned} \tag{4.16}$$

Once the posterior pdf is determined, it is straightforward conceptually to produce any desired statistic of $\mathbf{x}_k$.

Chapter 5

PERFORMANCE EVALUATION OF THE PROPOSED MAD SYSTEM

This chapter includes details simulation results to depicts the outcomes of our study. First we shall present an ocean environment which includes simulation parameters of the medium and induced magnetization of the ferromagnetic target due to earth's magnetic field in Sec. 5.1. Then we shall show the contribution of magnetic noise signals from different layer of the ocean which is the MAD signals in absence of the target in that area of search in Sec. 5.2. After that detection performance of the EMD method using tri-axial magnetometer will be presented in Sec. 5.3. Finally we will give simulation results of the classification, localisation and tracking performance of our proposed combined PF and UKF method in Sec. 5.4.

5.1 SIMULATION ENVIRONMENT

We have considered the underwater surveillance environment as a three layered medium (air-seawater-seafloor). The parameters for air medium (region 1) are: $\sigma = 0\mho$, $\mu = 1\mu_0$, $\epsilon = 1\epsilon_0$, for seawater medium (region 0) are: $\sigma = 4\mho$, $\mu = 1\mu_0$,

$\epsilon = 78\epsilon_0$, and for seabed medium (region -1) are: $\sigma = 0.1\mho$, $\mu = 1\mu_0$, $\epsilon = 12\epsilon_0$. Depth of the water region is $200m$.

Table 5.1: Equivalent Magnetic Moment of the Ferromagnetic Body due to the Magnetization in Earth's Magnetic Field

Ship Length $L\ (m)$	Ship Diameter $D\ (m)$	Tower Height $h\ (m)$	Tower Diameter $d\ (m)$	Equivalent Magnetic Moment $m\ (Am^2)$
100	10	2	2	$\simeq 10000$
55	10	2	2	$\simeq 5000$
70	6	2	2	$\simeq 4000$
28	6	No tower	No tower	$\simeq 1500$

In this study, the classification means the determination of the magnetic moment produced by the ferromagnetic target which leads to the determination of the target's size. To obtain the distribution of target's magnetization due to the external earth's magnetic filed, a ship built with a representative high strength steel is considered. For simplicity, the total body is assumed to be made of same material where the main body is of cylindrical shape and two hemisphere on two ends. The ship also has a tower on top, which is also cylindrical. Some numerical calculations are presented to depict a possible view of the induced magnetization of the ferromagnetic target in Table 5.1. Here, volume magnetic susceptibility of the steel, $\chi_v = 2.7$, thickness of the steel, $t_d = 4cm$, number of small volume element, n $\simeq 40000$, external magnetic field, $|\vec{\mathrm{B}}| = 55\ u\mathrm{T}$ are used for calculating induced magnetization.

5.2 ANALYSIS OF NOISE SIGNALS

A volumetric distribution of isolated elementary magnetic dipoles is considered to estimate the magnetic noise encountered by a MAD system. Time varying noise signals are generated by using the mathematical models developed in Sec. 3.1 to measure the magnetic fields due to a single magnetic dipole in the stratified media, and in Sec. 3.3 to measure the fields due to multiple dipoles considering dipole moments m, dipole frequencies f, orientations θ and initial phases ψ are random in nature. Two types of dipoles−horizontal magnetic dipole along-x direction and vertical magnetic dipole are considered as noise sources. Observation point P is at $10m$ above the air-water interface, and total number of dipoles is 50, which are distributed in the seawater within $(X, Y) = ([-10,\ 10], [-10,\ 10])m$ of the target following random distribution. Signals are observed within a time frame of $[0,\ 120]sec$. The parameter for dipoles are: magnetic moments, $m = rand[0.1,\ 1]Am^2$, frequency, $f = rand[0.1,\ 3]Hz$, orientation of the dipole with respect to x axis, $\theta = rand[0,\ 360^0]$ and initial phase, $\psi = rand[0,\ 2\pi]$.

Figure 5.1 shows the noise signals for the Noise Source Layer (NSL) $[0.01,\ 0.1]m$, which means the dipole sources are distributed $0.01m$ to $0.1m$ below the air-seawater interface. The magnetic fields are plotted along three axes to correspond with the detection technique of Three-Axis Magnetometer.

Attenuation of EM fields is very high due to the large electric conductivity ($\sigma = 4\ to\ 5\mho$) and electric permittivity ($\varepsilon \simeq 80\varepsilon_0$) of the seawater. Magnetic fields due to the dipoles distributed at near the interface are of high values, and fields contribution gradually diminishes with the increase of NSL from the interface. Considerable decreases in field strength are seen from Fig. 5.2 (NSL = $[9,\ 12]m$), and Fig. 5.3

(NSL $= [35,\ 40]m$). So, noise sources distributed at $[0.01,\ 40m$ from the air-seawater interface are of interest.

By inspecting the histogram chart and probability density of noise signals from Fig. 5.4 we can see the distribution as Gaussian distribution. So, we can assume the background environmental magnetic noise in ocean as Gaussian additive noise.

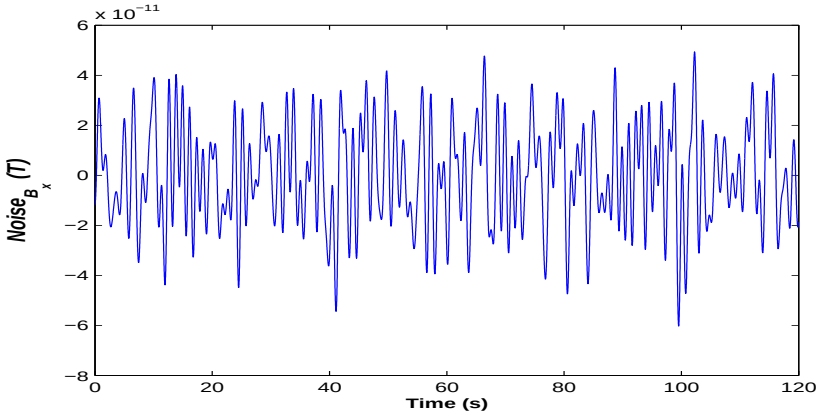

(a) Magnetic Noise: $x-$component

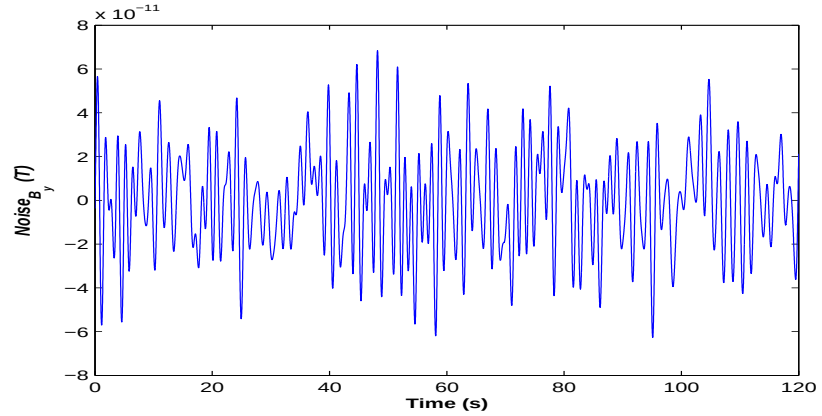

(b) Magnetic Noise: $y-$component

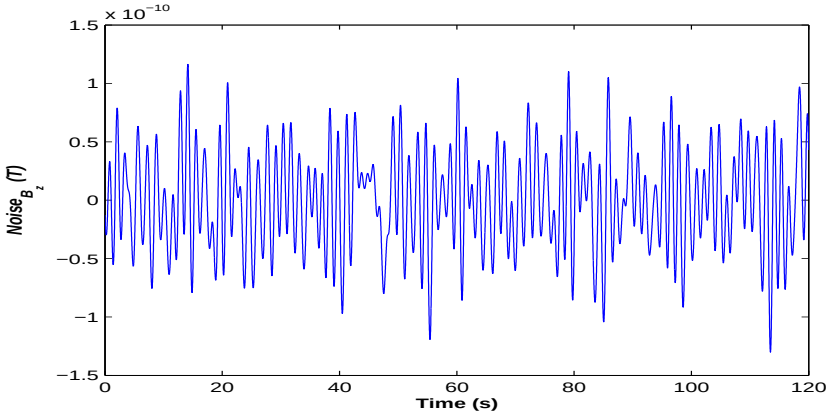

(c) Magnetic Noise: $z-$component

Figure 5.1: Magnetic Noise Signals due to NSL $([0.01, 0.1])m$

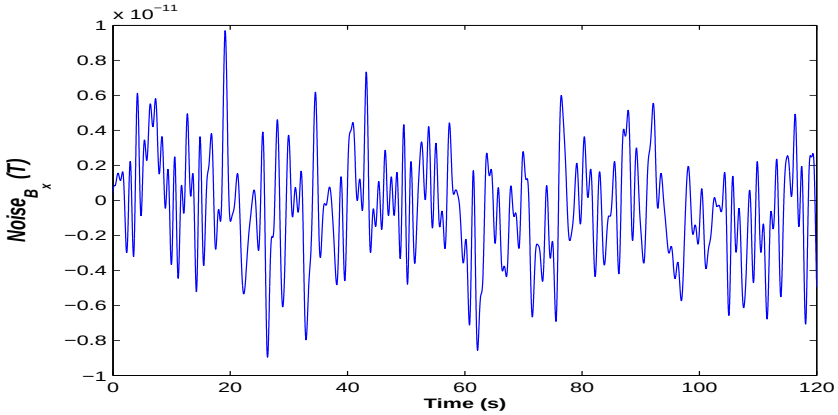

(a) Magnetic Noise: $x-$component

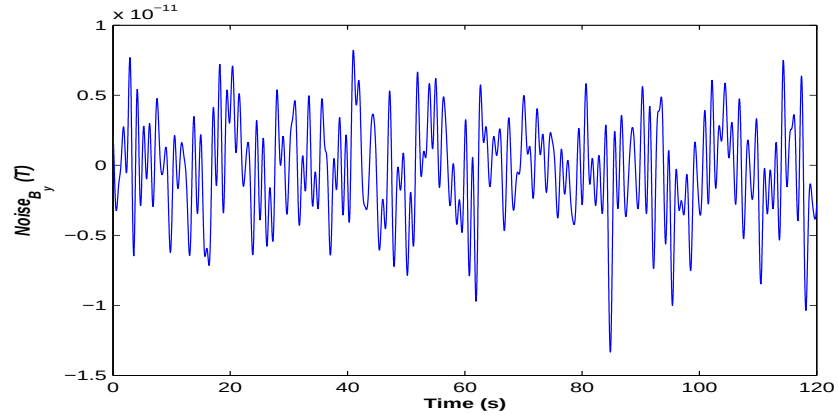

(b) Magnetic Noise: $y-$component

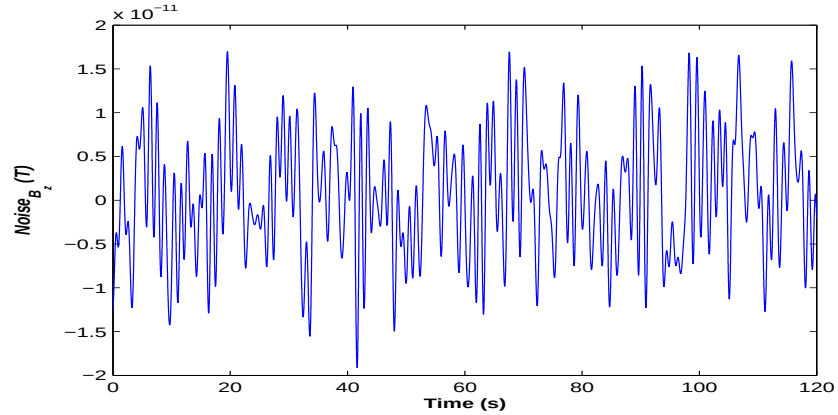

(c) Magnetic Noise: $z-$component

Figure 5.2: Magnetic Noise Signals due to NSL ([9, 12])m

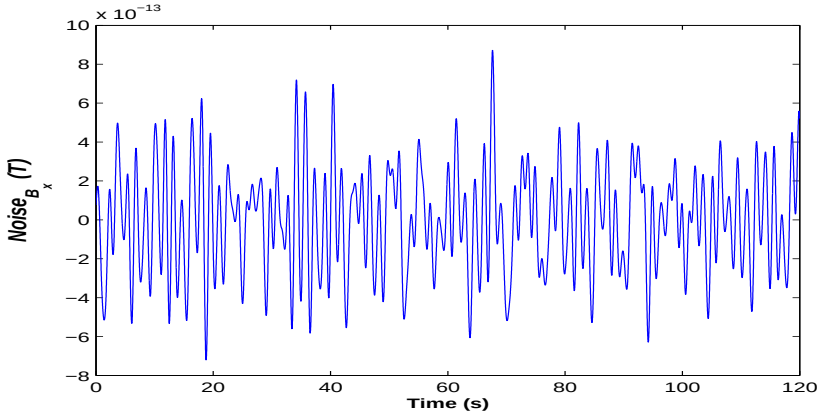

(a) Magnetic Noise: $x-$component

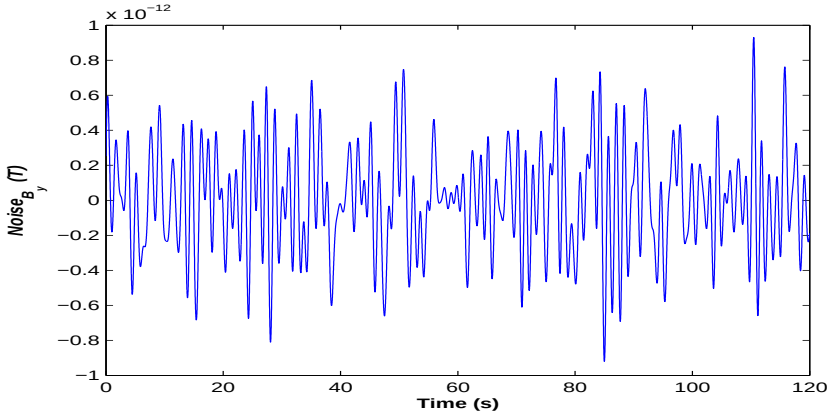

(b) Magnetic Noise: $y-$component

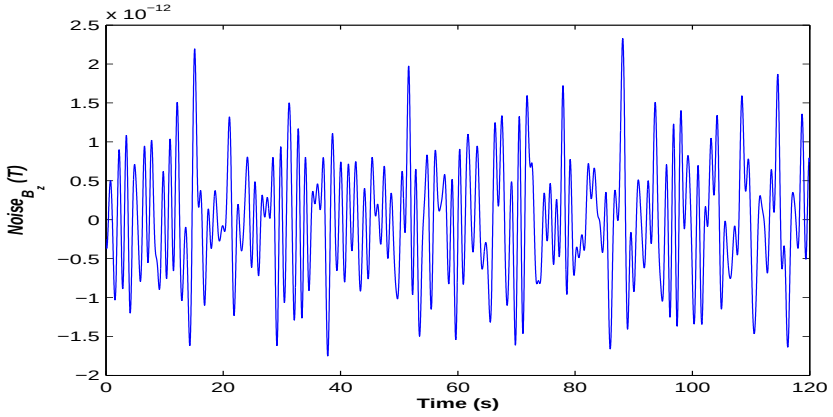

(c) Magnetic Noise: $z-$component

Figure 5.3: Magnetic Noise Signals due to NSL ($[35, 40]$)m

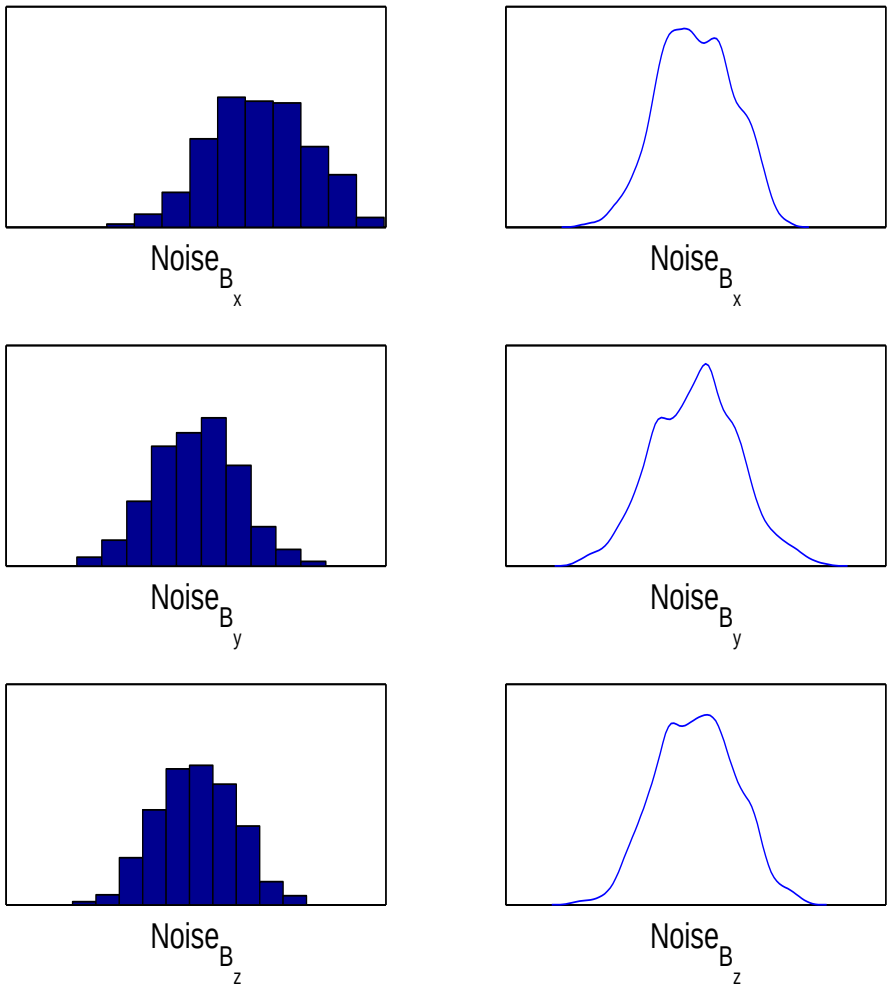

Figure 5.4: Histogram and Probability Density of the Noise Signals

5.3 DETECTION PERFORMANCES

EMD and hurst analysis [30] techniques are exploited to process the received EM signals of MAD sensor for detection purpose in this study. As using EMD in denoising is to decompose the noisy signal into the IMFs and Residue, and some IMFs contain useful signal information while others carry signal plus noise, the selection of proper number of IMFs is an important factor. Here, maximum number

of sifting iterations for the computation of each mode is 2000, and maximum number of IMFs extracted is infinite. Vector of stopping parameters is, $[\tau,\ \tau_2,\ tol] = [0.05,\ 0.5,\ 0.05]$. After decomposing the signal into IMFs and residue, it is seen that only first 4 to 5 IMFs are necessary for reconstructing the denoised signals. The threshold condition for successful detection from the figure is: the highest peak must be 20% greater than the mean peak value and 35% greater than the third peak value.

Figure 5.5 shows the $x,\ y,\ z$ components of the observed magnetic fields and their corresponding magnetic anomaly detected by EMD technique, where a horizontal magnetic dipole along-x direction having magnetic moment of 3 kAm^2 is present as a target, and 100 elementary small dipoles are present as noise sources. Target signals are of 3 Hz frequency, velocity is constant at 2 m/s, sampling frequency is 60 Hz and data analysis window is 30 seconds. The target follows the trajectory along the x direction of the search path with no heading to y axis at a constant depth of $70m$ below the air water interface, and there is no field due to the target at y axis magnetometer, only noise contribution, which is depicted in Figs. 5.1b and 5.5d. On the otherhand large anomalies are visible in observed magnetic fields of both x and z axis magnetometers, and target is easily detected from denoised signal after EMD analysis.

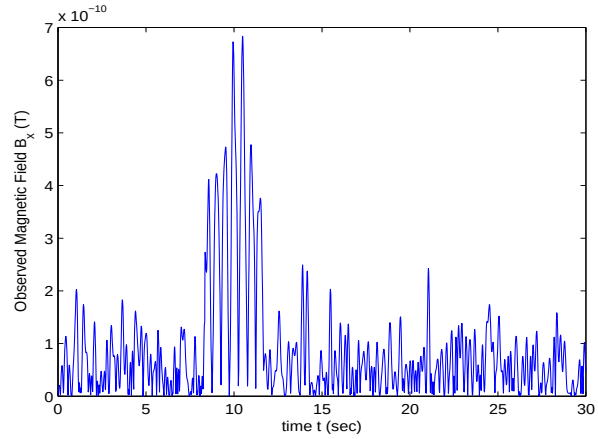

(a) Noisy Magnetic Field: $x-$component

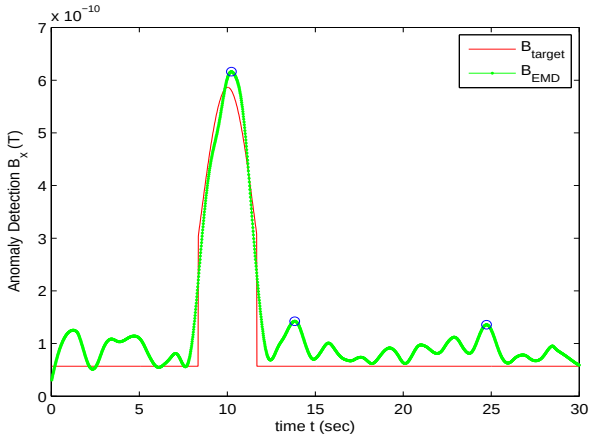

(b) Denoised Magnetic Field: $x-$component

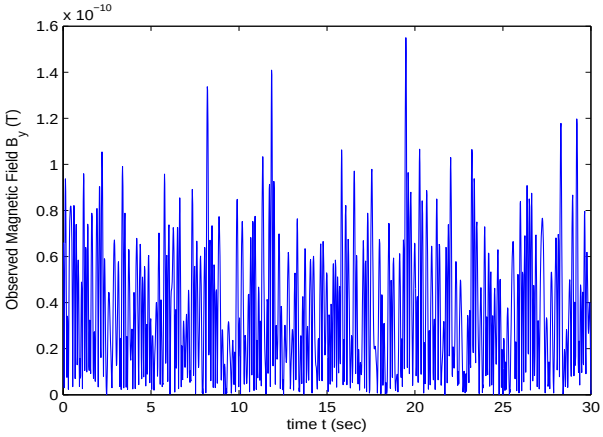

(c) Noisy Magnetic Field: $y-$component

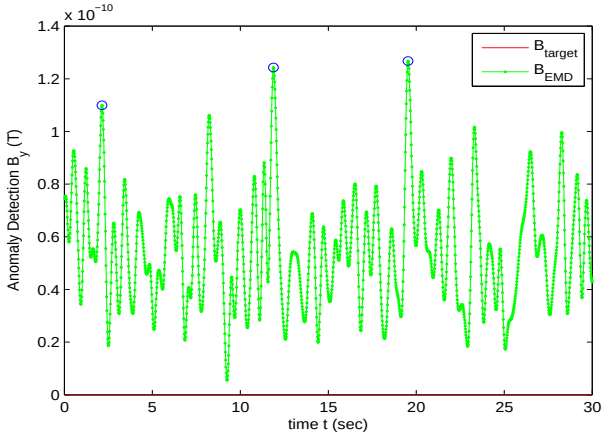

(d) Denoised Magnetic Field: $y-$component

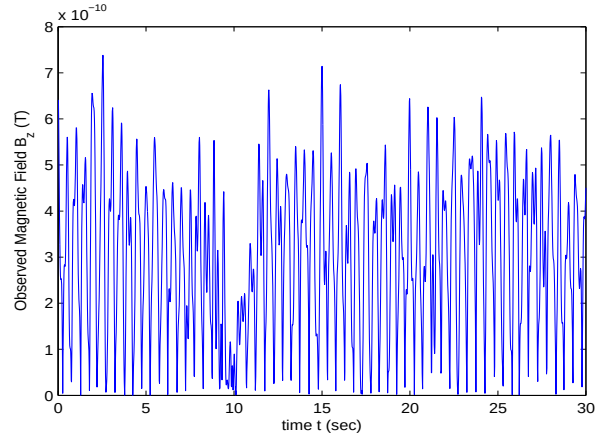

(e) Noisy Magnetic Field: $z-$component

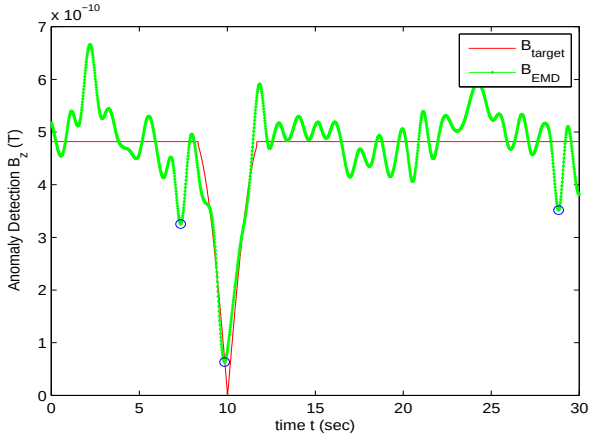

(f) Denoised Magnetic Field: $z-$component

Figure 5.5: Magnetic Anomaly When Target Has No Heading to y axis

Figure 5.6, shows the $x,\ y,\ z$ components of the observed magnetic fields and their corresponding magnetic anomaly detected by EMD technique for the same target having magnetic dipole moment of 3 kAm^2 moving at a constant depth of 70 m below the air-water interface. But the target follows the trajectory keeping 30 degree heading with x direction of the search path. So, we get the field contribution due to target in y axis magnetometer, which is also detected after denoising.

Signal strength depends on size of the target and on distance of the target which are the important factors for detection system. If the target is very small or the depth is very high then the system fails to detect the target. Figures 5.7a, 5.7c, 5.7e are for a small target of $500Am^2$ moment following the same trajectory at a constant depth of $70m$ like Fig. 5.6. Similarly, Figs. 5.7b, 5.7d, 5.7f are for the same target of $3kAm^2$ like Fig. 5.6 following the trajectory at a large constant depth of $120m$. In both of the cases, system fails to detect the target.

But the target can be detected if it's trajectory is near to the surface for small target or if it's size is large enough for long distance from the surface. Figures 5.8a, 5.8c, 5.8e are for the small target of $500Am^2$ moment following the trajectory at a constant depth of $30m$ while Figs. 5.8b, 5.8d, 5.8f are for the large target of $8kAm^2$ following the trajectory at the constant depth of $120m$. In both of the cases, performances of the system improve.

Sometimes, the target's trajectory crosses the search path of the sensor for small period of time. Our system can detect the target in that case also shown in Fig. 5.9.

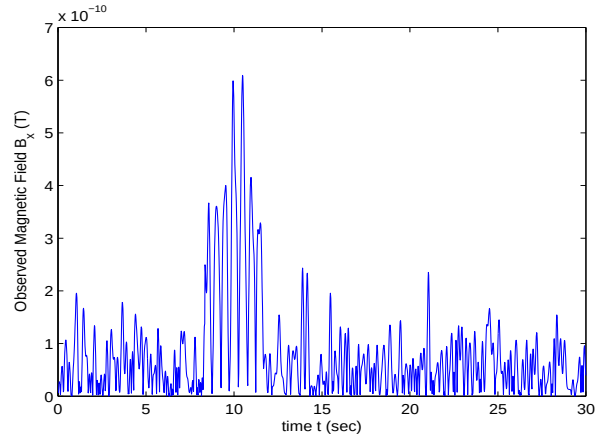

(a) Noisy Magnetic Field: $x-$ component

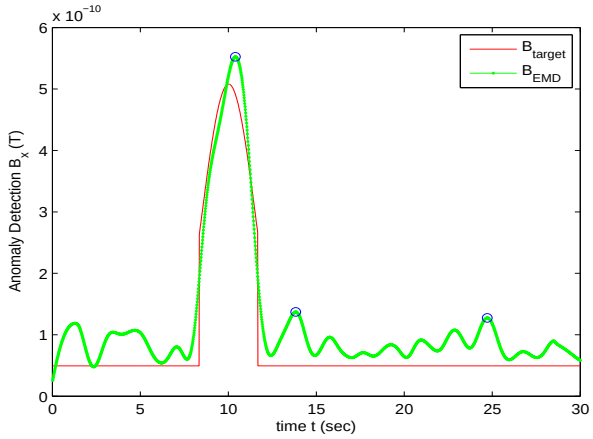

(b) Denoised Magnetic Field: $x-$component

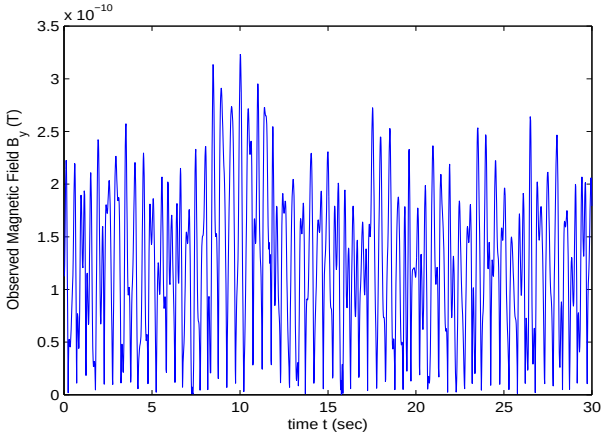

(c) Noisy Magnetic Field: $y-$component

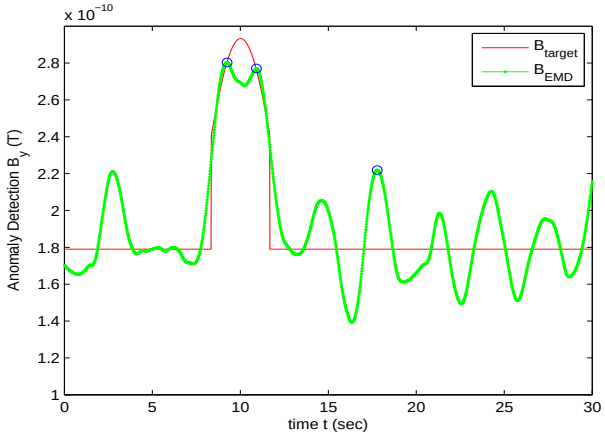

(d) Denoised Magnetic Field: $y-$component

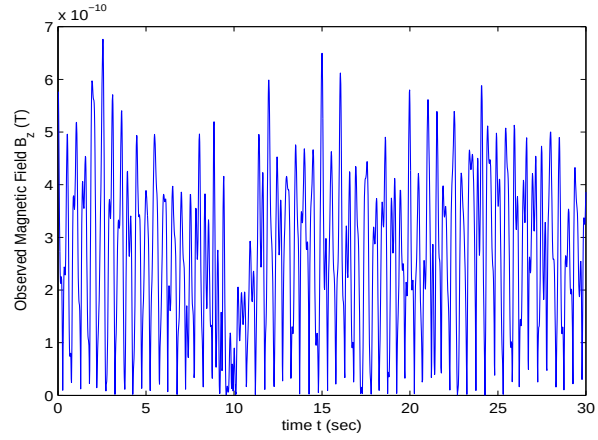

(e) Noisy Magnetic Field: $z-$component

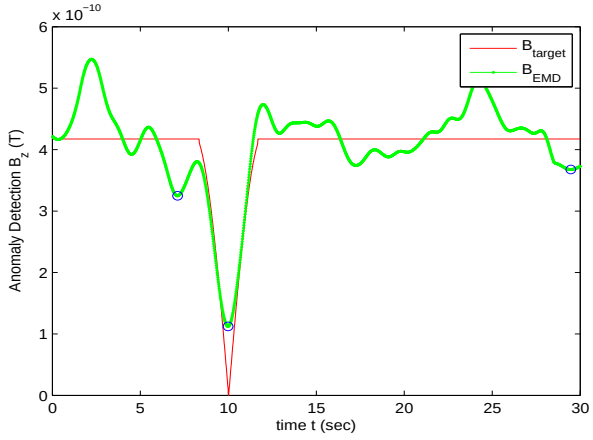

(f) Denoised Magnetic Field: $z-$component

Figure 5.6: Magnetic Anomaly When Target Follows 30 degree Heading to y axis

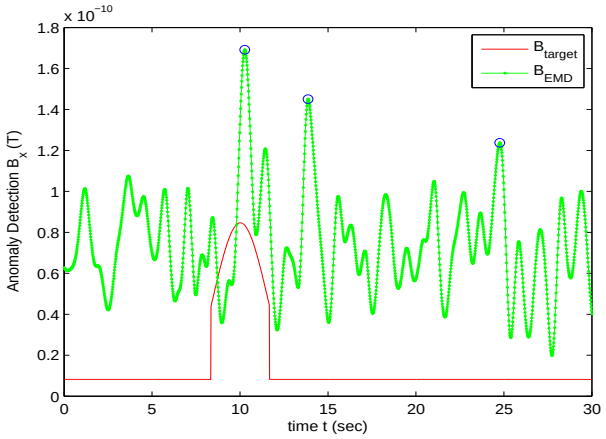

(a) Small Target: denoised $x-$ component

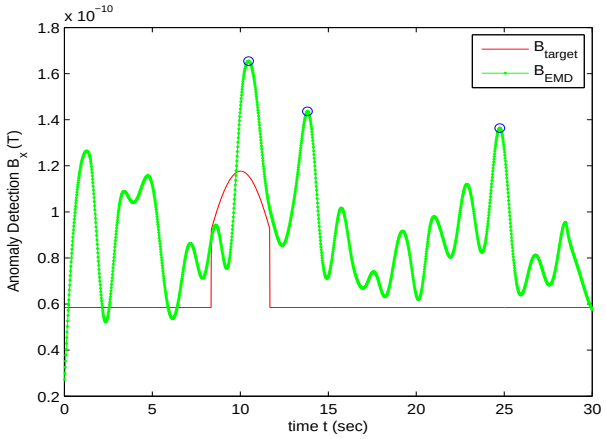

(b) Large Depth: denoised $x-$component

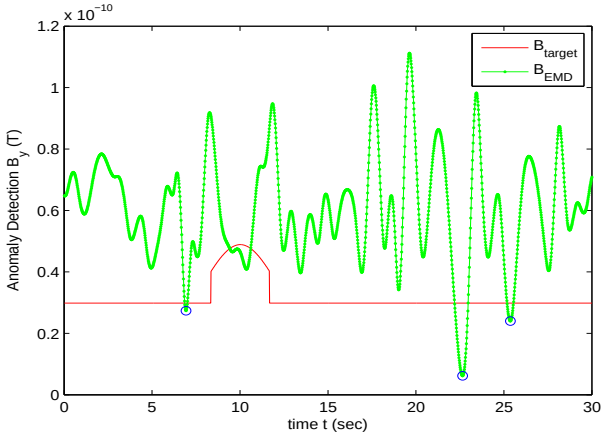

(c) Small Target: denoised $y-$component

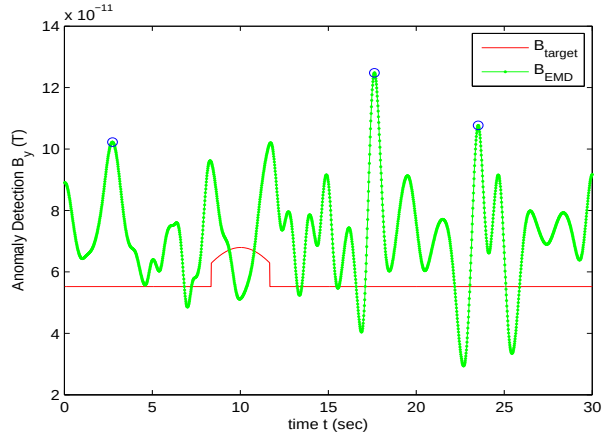

(d) Large Depth: denoised $y-$component

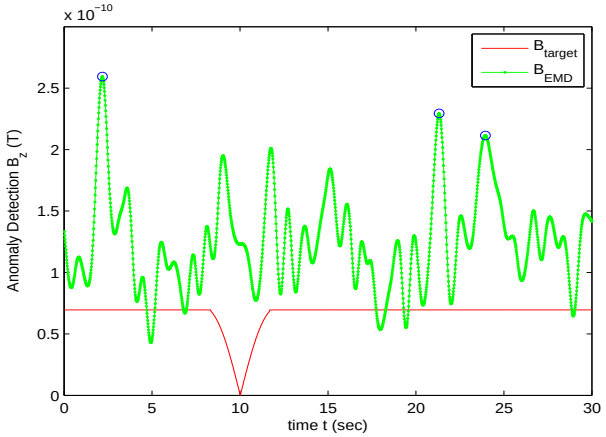

(e) Small Target: denoised $z-$component

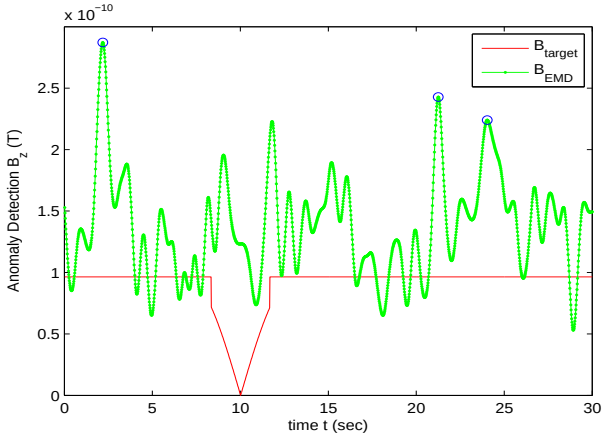

(f) Large Depth: denoised $z-$component

Figure 5.7: Detection Failure Due to Small Target or Large Depth

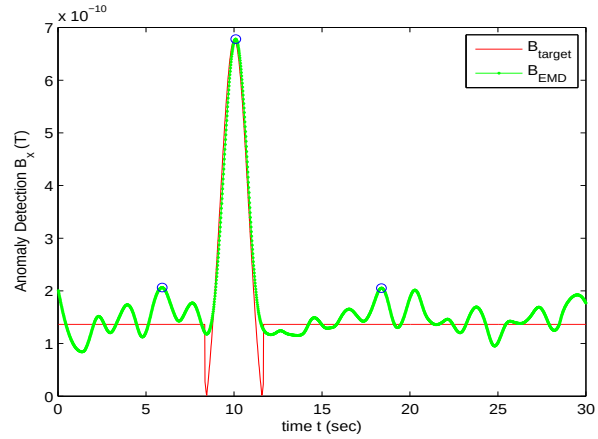

(a) Small Depth: denoised $x-$ component

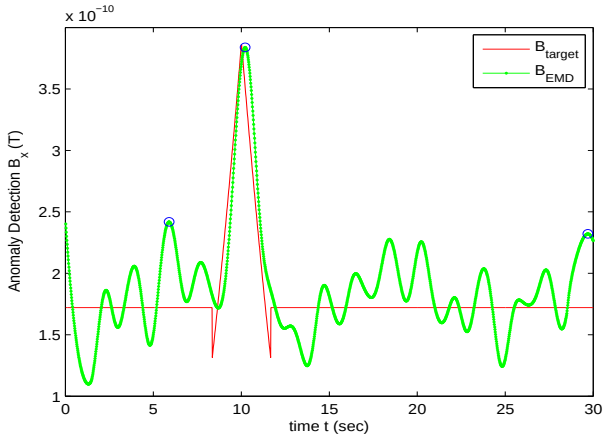

(b) Large Target: denoised $x-$component

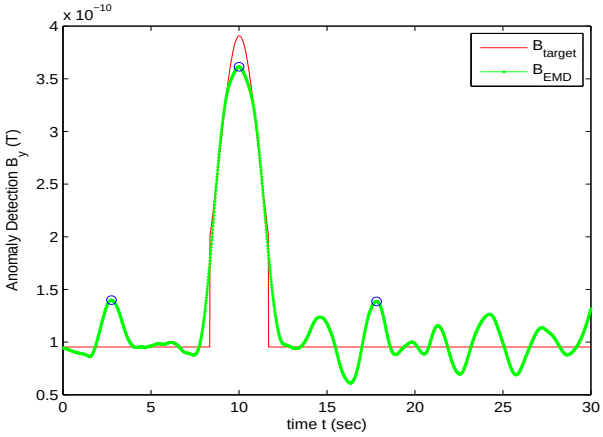

(c) Small Depth: denoised $y-$component

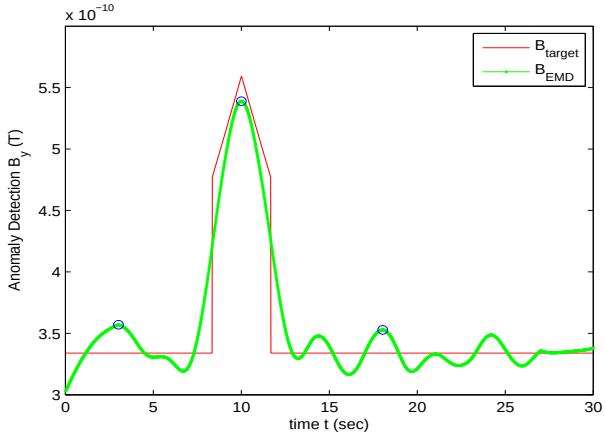

(d) Large Target: denoised $y-$component

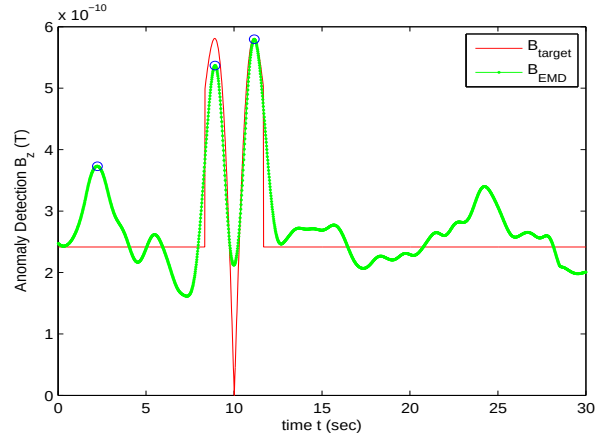

(e) Small Depth: denoised $z-$component

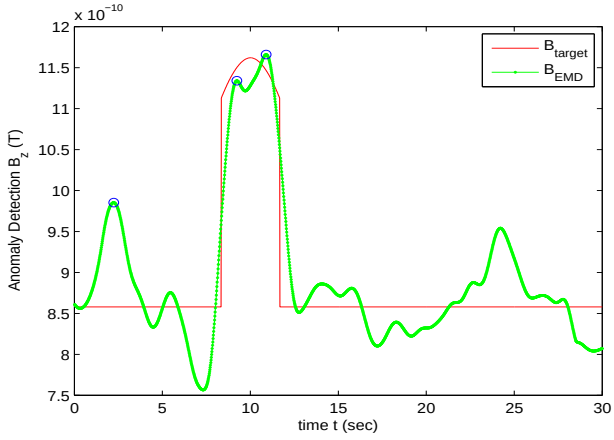

(f) Large Target: denoised $z-$component

Figure 5.8: Successful Detection If Trajectory is Near the Surface or Target is Large

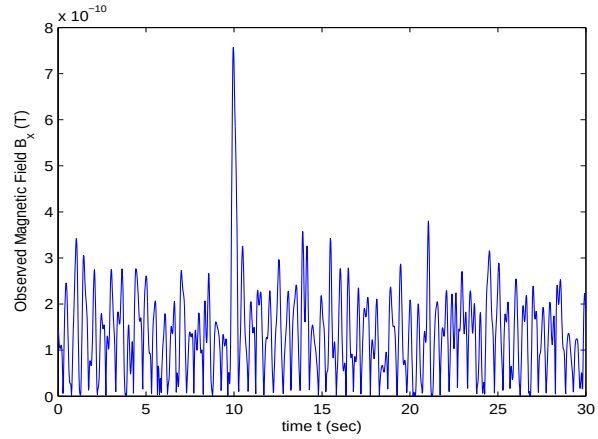

(a) Noisy Magnetic Field: $x-$component

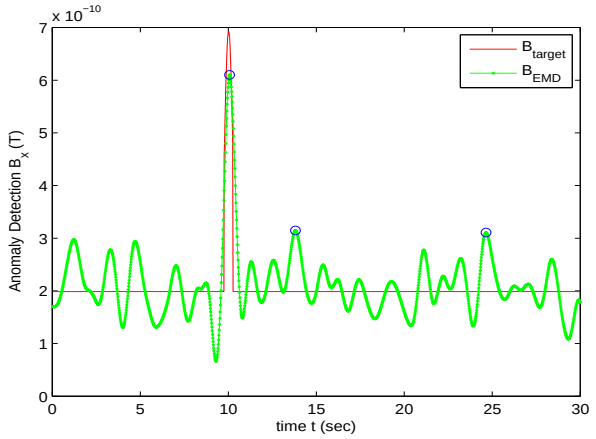

(b) Denoised Magnetic Field: $x-$component

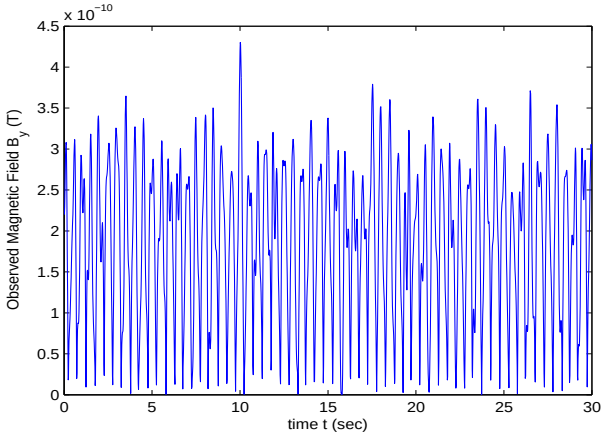

(c) Noisy Magnetic Field: $y-$component

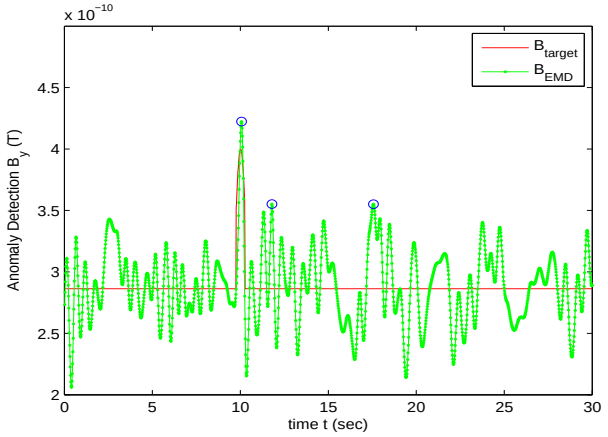

(d) Denoised Magnetic Field: $y-$component

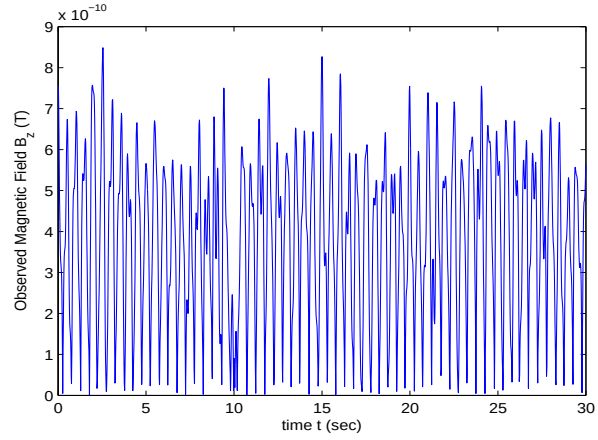

(e) Noisy Magnetic Field: $z-$component

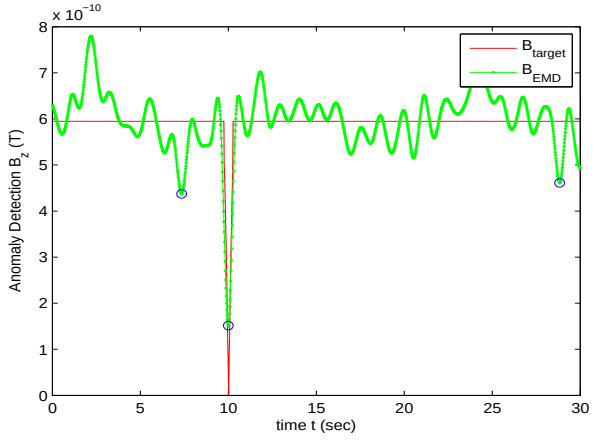

(f) Denoised Magnetic Field: $z-$component

Figure 5.9: Magnetic Anomaly Presented for a Small Period of Time

5.4 CLASSIFICATION, LOCALISATION AND TRACKING PERFORMANCES

A triangular (Fig. 5.10) and a pyramid (Fig. 5.11) geometry of sensors position in air, moving target in water region, distributed myriad of noise sources are used to perform the tracking simulations. Observer sensor's positions are S1(0, 2, 5), S2(0, -2, 5), S3($2\sqrt{3}$, 0, 5), S4(-$2\sqrt{3}$, 0, 5) and S5(0, 0, 9). That means observers are 5 m above the air-water interface except S5, which is 9 m above the interface, assuming the coordinate is at the interface. In triangular geometry sensors S1, S2 and S5 are used, and in pyramid geometry all the sensors are used. Some measurements are also shown for linear sensor geometry (S1 ans S2 sensors in 2-sensors system).

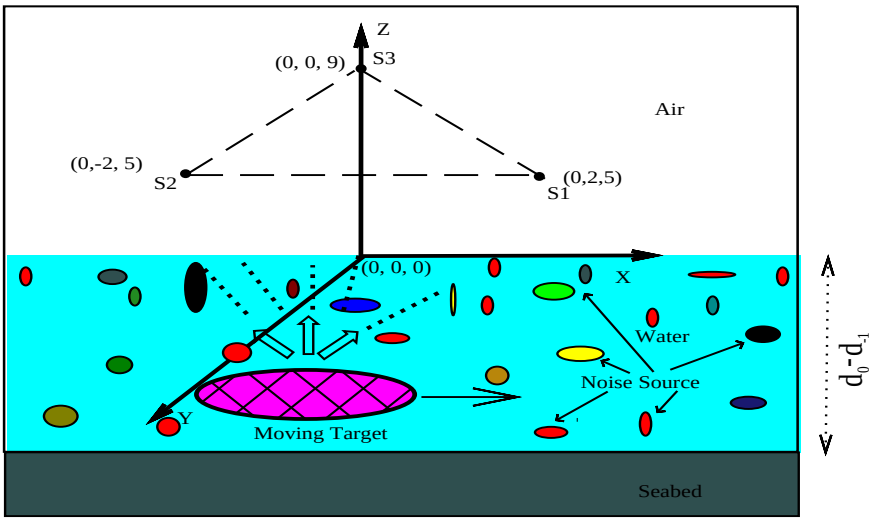

Figure 5.10: Schematic of a 3-sensors Tracking System

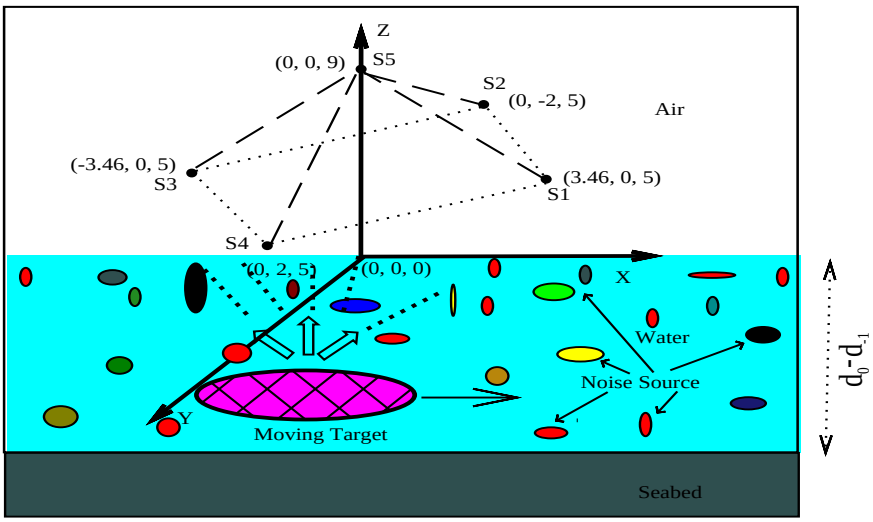

Figure 5.11: Schematic of a 5-sensors Tracking System

UKF depends largely on initialising of the parameters. So, simultaneous optimization of magnetic moment and dipole position are not satisfactory. In this thesis, Particle filter [31] is used to estimate the initial value of the target's parameters such as magnetic moment and initial localisation of the position of the target. After that UKF [32] is used for tracking the trajectory of moving dipole as UKF is the best suited algorithm for non-linear dynamic system. In Particle Filter, Five particles are generated around initial values of each of the position states $X,\ Y,\ and\ Z$, which results $5^3 = 125$ particles after permutation among themselves. The fourth and fifth states are velocity states $V_X,\ V_Y$, which are assumed from the position states. For sixth state, which is the magnetic moment of the target, 15 random numbers are generated from the normal distribution. Observation are done for these magnetic moments at each of the position states, which means total number of particles are 1875. After the single iteration of the Particle Filter, the output is used as the initial states for the UKF. It updates state vector and covariance matrix

in every iteration. As signal strength depends strongly on the distance between the sensors position and the target, for continuous tracking of the trajectory sensor platform is moving at updated estimated velocity after $20secs$ following the search path.

In applying the filtering to the system, the initial conditions and the noise covariance matrixes need to be specified. As detection is done previously, we may guess horizontal position roughly. For the vertical position, an initial estimate between zero and the approximate water depth can be given. Because no information is available about the magnitude of velocity and magnetic dipole moments, a good initial estimate of these vectors are merely the null vectors. So, the initial state vector is:

$$x_0 = [\simeq r_X,\ \simeq r_Y,\ 0 \sim r_Z,\ 0,\ 0,\ 0]$$

The initial estimates of the variance affect the transient performance of the algorithm and the choice of the appropriate values will prevent filter divergence. Small values for initial variances give large values of filter gain meaning that the initial observations are heavily weighted and the model is ignored. On the other hand, too large variance values make the filter gain extremely small and the algorithm diverges. The initial covariance matrix, $\mathbf{P}(0|0)$ is assumed that initially all the states are un-correlated, so that the matrix is diagonal. So, the diagonal components of variance matrix is:

$$\mathbf{P}_{diag} = [0.25^2,\ 0.25^2,\ 0.5^2,\ 2^2,\ 2^2,\ 10^2]$$

The measurement noise covariance matrix can be estimated directly from the actual data and the process noise covariance is assumed small (10^{-4}). In UKF,

higher order error scaling parameter is 2, and sigma points scaling for weighting unscented transformation is 10^{-3}.

To generate the true trajectory of a target, a horizontal magnetic dipole along x direction is assumed. The target is moving at different constant velocity to different directions at constant depth assuming the trajectory is linear and there is no vertical velocity. Both simple white Gaussian noise ($SNR = 20dB$), and our proposed noise model (50 elementary small dipoles) are used to generate the noise signals which ensembles the practical ocean environment. Discrete observations are taken at a sampling period of one second for total travel time of 2 minutes. Table **??** presents the summary of the simulation results for different cases.

Figures 5.12 and 5.13 depicts the localisation and tracking performances of 2, 3 and 5 sensors systems using UKF filtering technique when magnetic moment is known that is no need for classification. From Fig.5.12a, it is seen that every system can satisfactory track the x trajectory of the moving target. In tracking y trajectory 3 sensors system is closest than other sensor systems and 2 sensor system has largest offset from true trajectory.

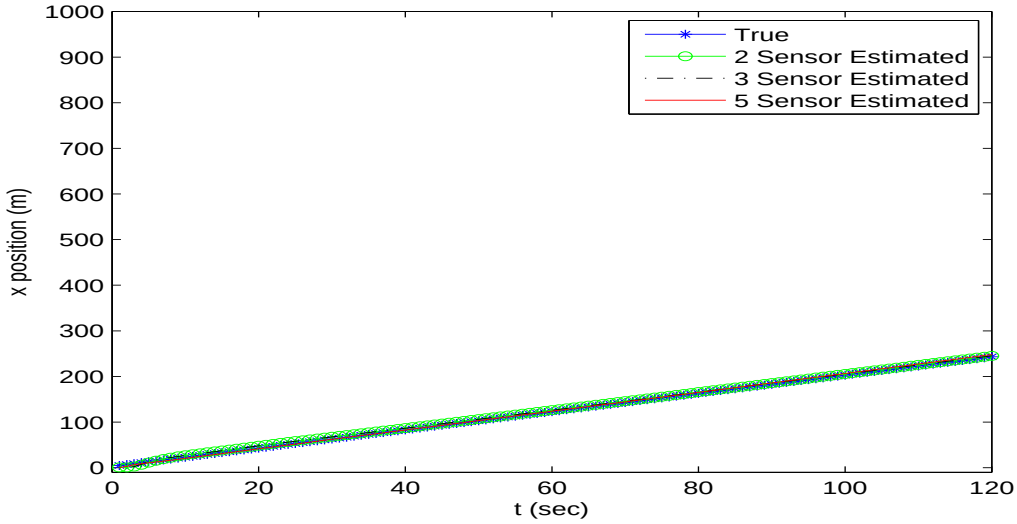

(a) $x-$ trajectory tracking

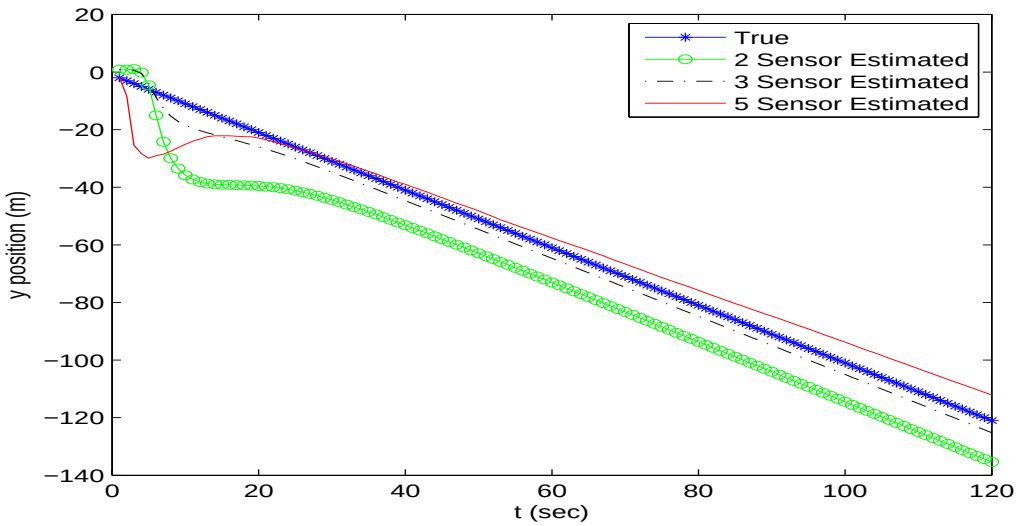

(b) $y-$ trajectory tracking

Figure 5.12: Performances in Trajectory Tracking of 2, 3 and 5 Sensors Systems When m is Known

Figure 5.13a shows that all the systems have small error in velocity estimation. 5 sensor system is successful in localising depth of the target while 3 sensor system

performs in acceptable level depicted in Fig. 5.13b.

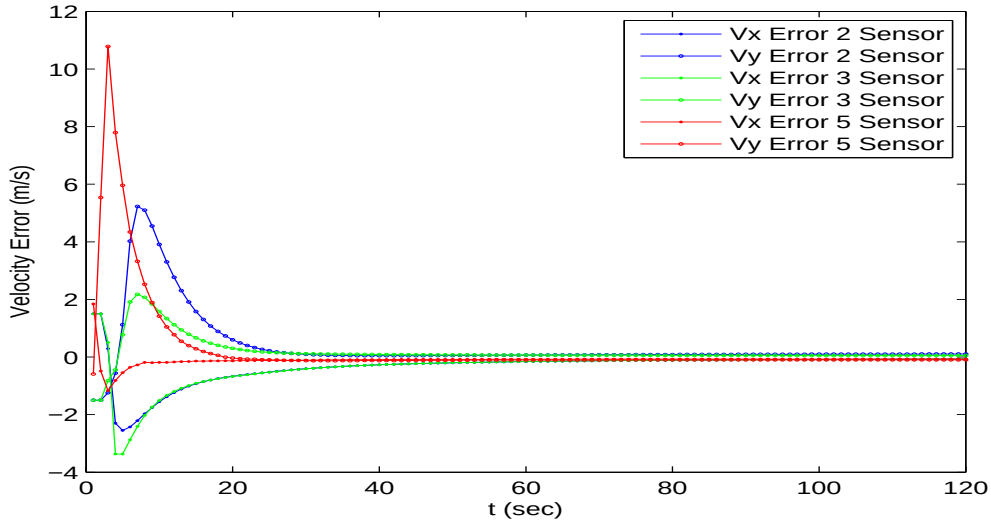

(a) Velocity tracking

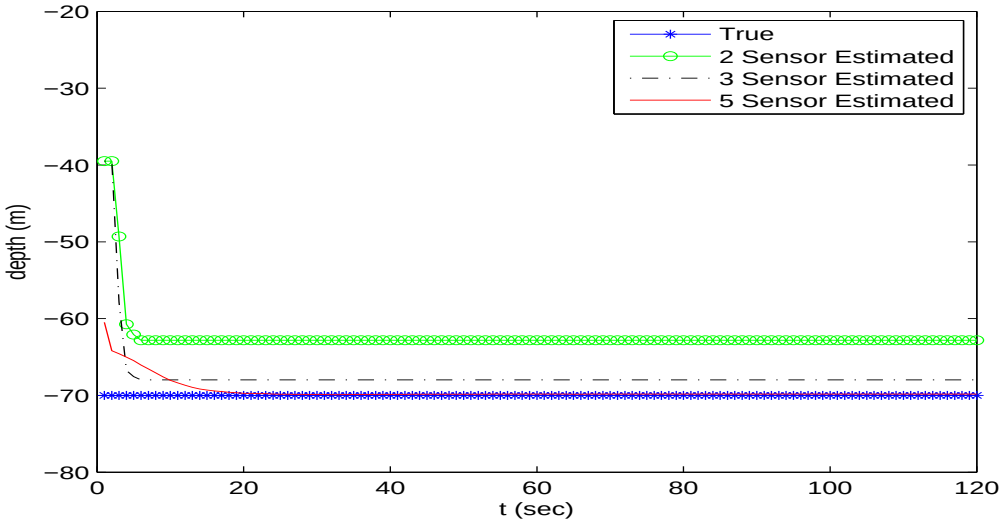

(b) Depth tracking

Figure 5.13: Performances in Velocity Tracking and Depth Localisation of 2, 3 and 5 Sensors Systems When m is Known

Figures 5.14, 5.15 and 5.16 are the performances comparison of 2, 3 and 5 sensor

systems using UKF filtering technique when classification is also necessary. From Figs. 5.14a and 5.14b, it is seen that 5 sensor system tracks the trajectory in acceptable limit while others fail.

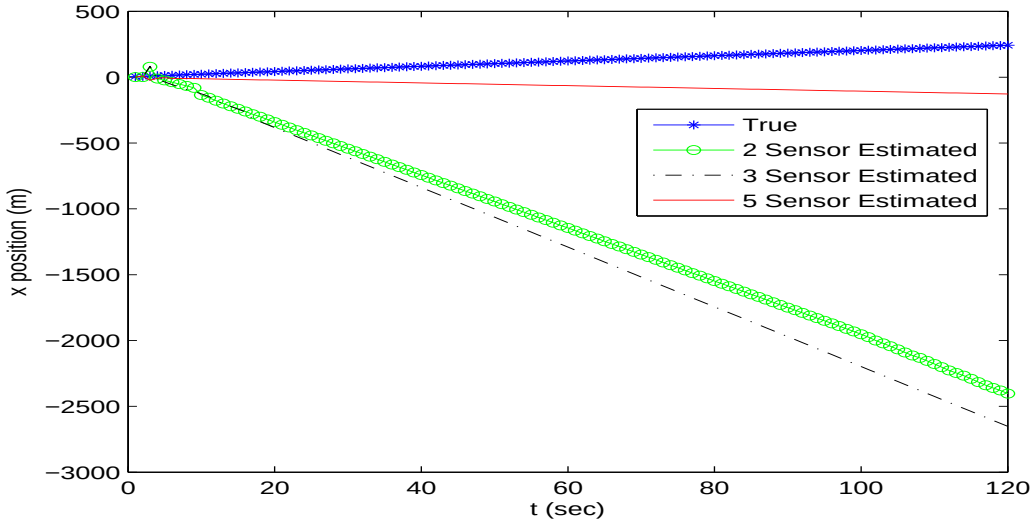

(a) $x-$ trajectory tracking

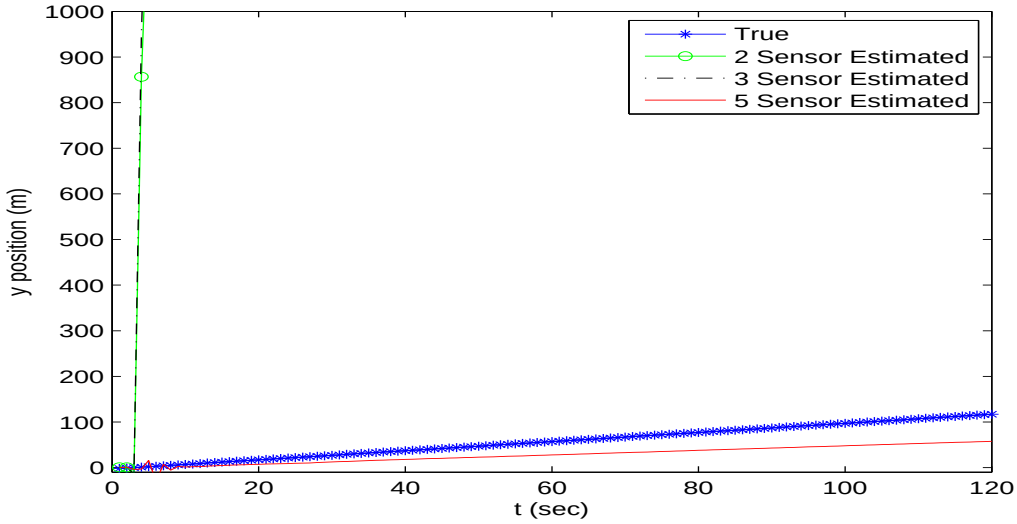

(b) $y-$ trajectory tracking

Figure 5.14: Performances in Trajectory Tracking of 2, 3 and 5 Sensors Systems When m is Unknown

Figure 5.15a shows that velocity error is small for 5 sensor system while large velocity errors are occurred in y axis of 2 and 3 sensor systems. No system can perform localisation of depth of the target in acceptable level shown in Fig. 5.15b.

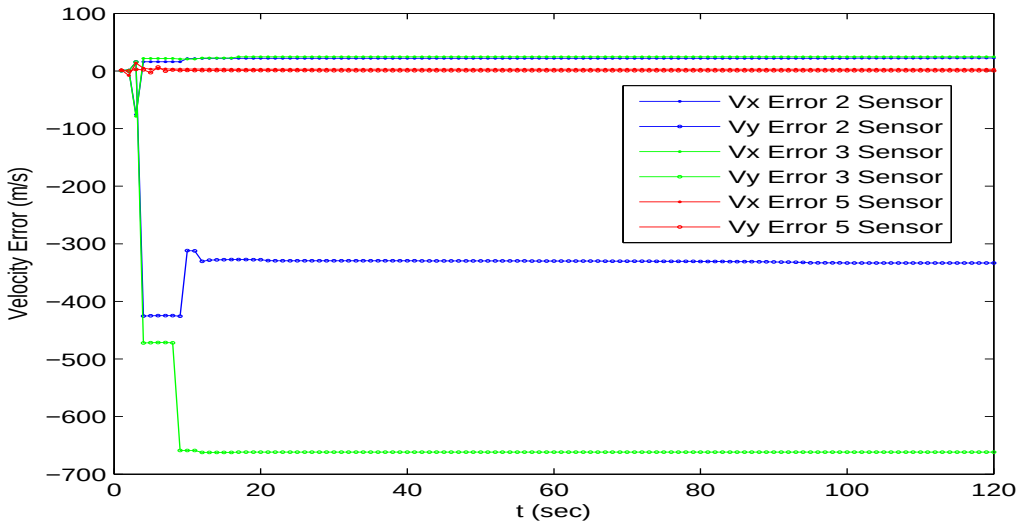

(a) Velocity tracking

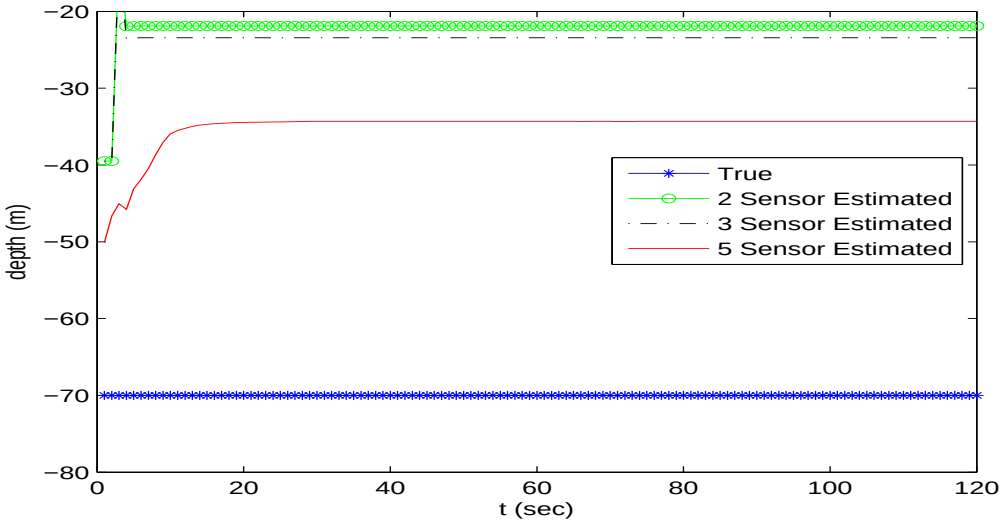

(b) Depth tracking

Figure 5.15: Performances in Velocity Tracking and Depth Localisation of 2, 3 and 5 Sensors Systems When m is Unknown

Figure 5.16 depicts that all system fail in estimating the target's magnetic moment.

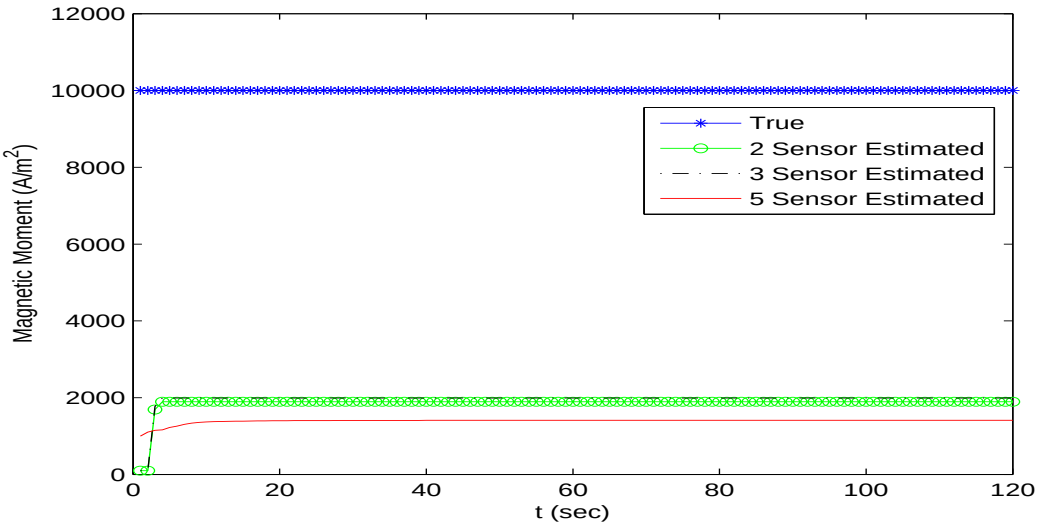

(a) Magnetic moment estimation

Figure 5.16: Performances in Classification of 2, 3 and 5 Sensors Systems When m is Unknown

So, new filtering technique is necessary for satisfactory performances. Figures 5.17, 5.18 and 5.19 show the performance comparison of different filtering techniques such as only PF, only UKF and combined PF and UKF.

Figure 5.17a and 5.17b show that in tracking the trajectory only UKF fails, only PF gives acceptable result while combined PF and UKF performs satisfactorily.

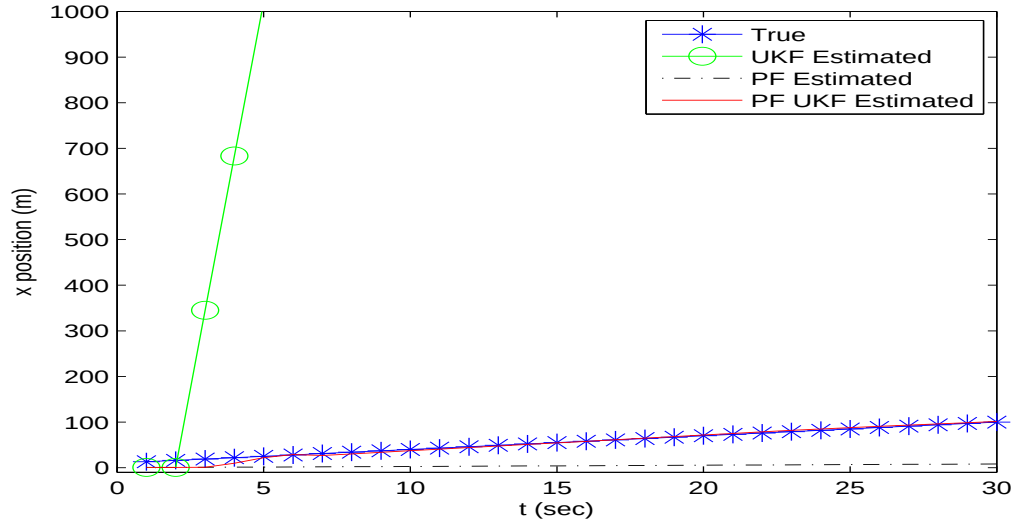

(a) $x-$ trajectory tracking

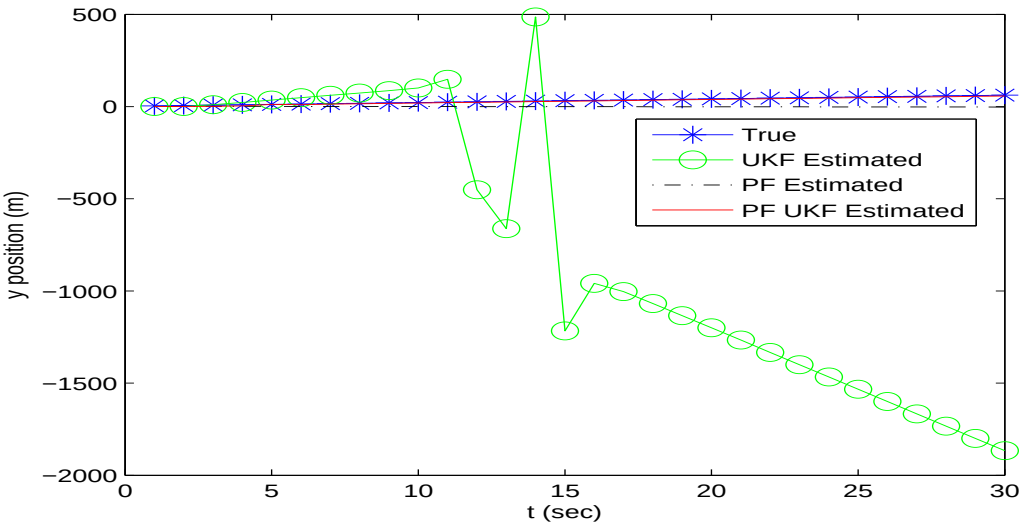

(b) $y-$ trajectory tracking

Figure 5.17: Performances in Trajectory Tracking of Different Filtering Techniques

From Fig. 5.18a it is seen that only UKF fails in velocity tracking. In localising the depth of the target combined PF and UKF is successful shown in Fig. 5.18b.

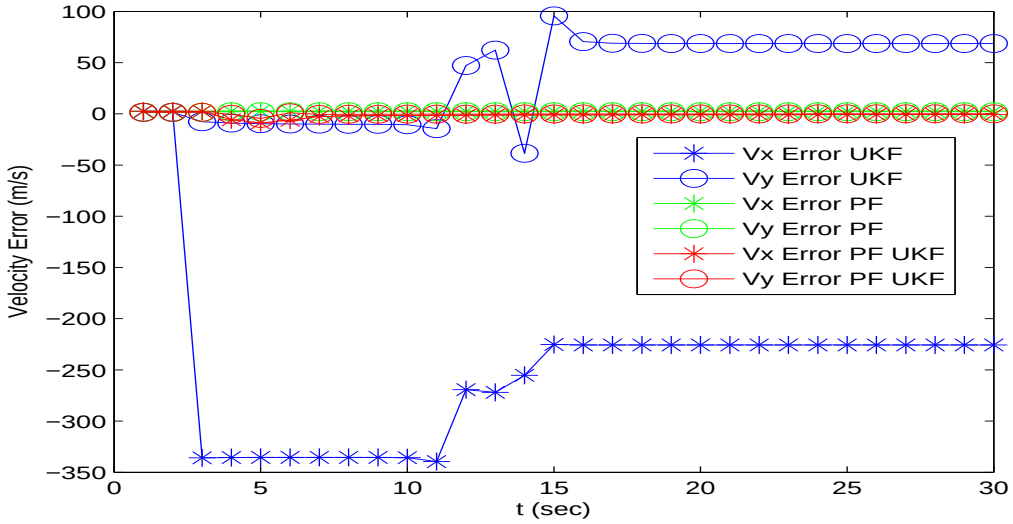

(a) Velocity tracking

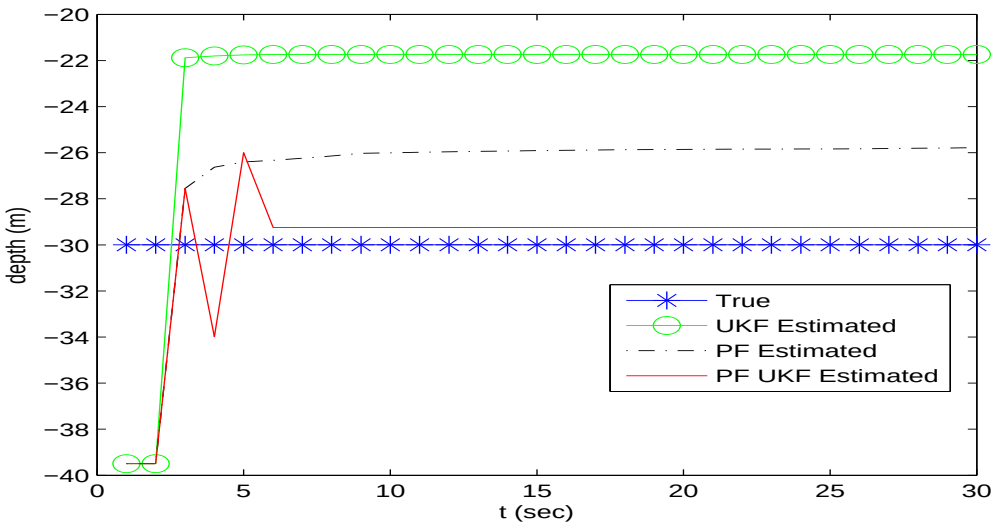

(b) Depth tracking

Figure 5.18: Performances in Velocity Tracking and Depth Localisation of Different Filtering Techniques

Figure 5.19 shows that only UKF performs in acceptable level while combined PF and UKF performs satisfactorily in estimating the target's magnetic moment. So,

the proposed combined PF and UKF filtering technique is successful in classification, localisation and tracking the target.

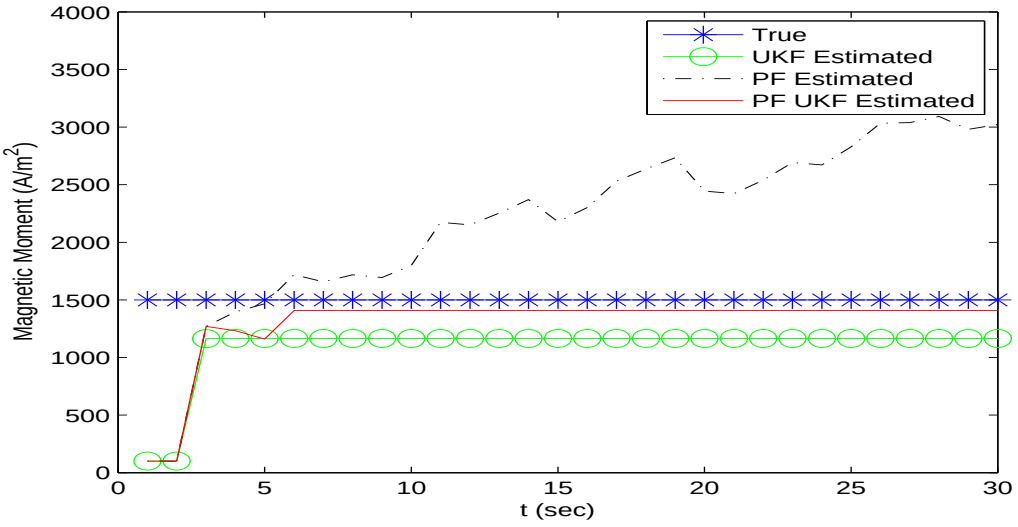

(a) Magnetic moment estimation

Figure 5.19: Performances in Classification of Different Filtering Techniques

Range of the localization of a MAD system depends on signal's strength. The signal strength will be small if the target is not large enough but depth is very large and system will fail. But if the target's size is large enough to produce signal in good strength, then the proposed method still perform the task. From Figs. 5.20, 5.21 and 5.22, it is seen that when a medium sized target having magnetic moment $5kAm^2$ moves $100m$ below the interface then system fails in trajectory and velocity tracking although depth localisation and classification are in acceptable level. But if target is large having magnetic moment $10kAm^2$ then the proposed system can perform total classification, localisation and tracking.

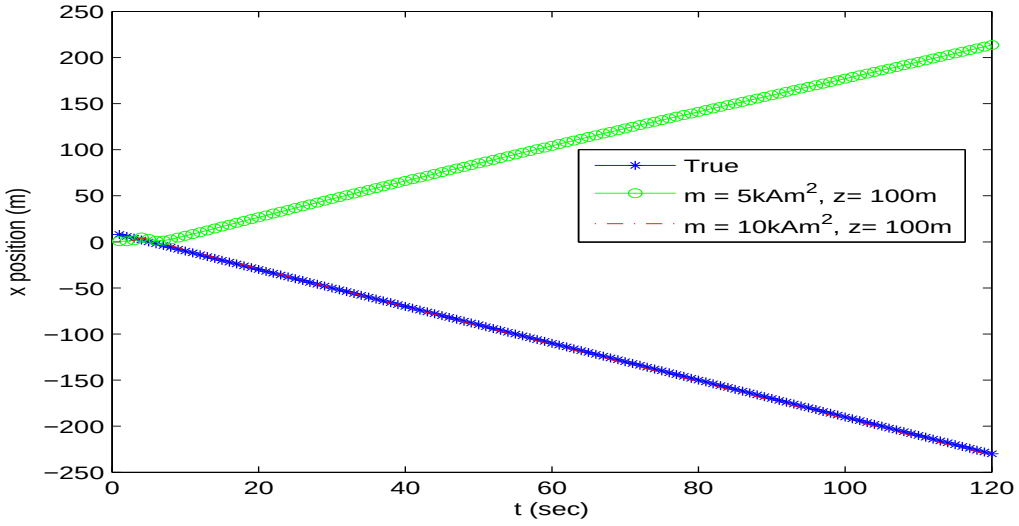

(a) $x-$ trajectory tracking

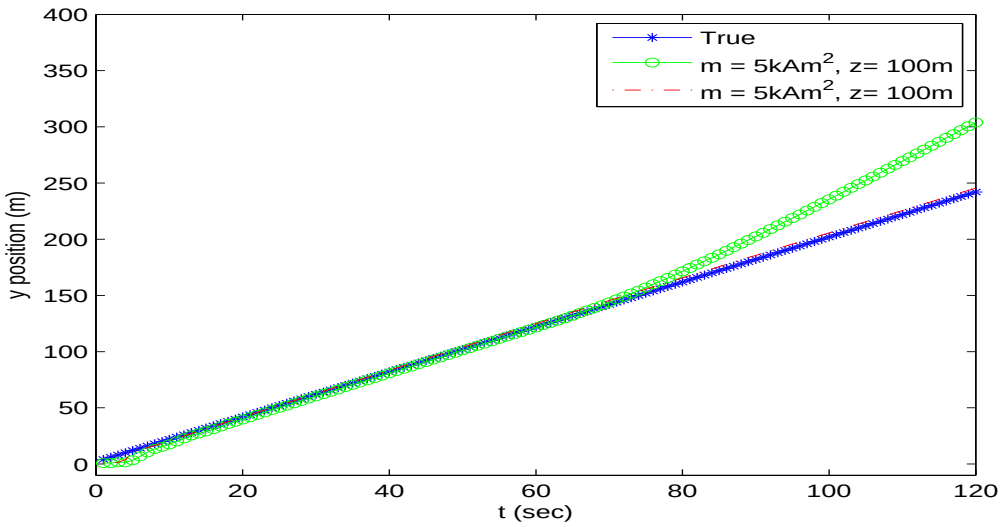

(b) $y-$ trajectory tracking

Figure 5.20: Performances in Trajectory Tracking Considering Range of Detection

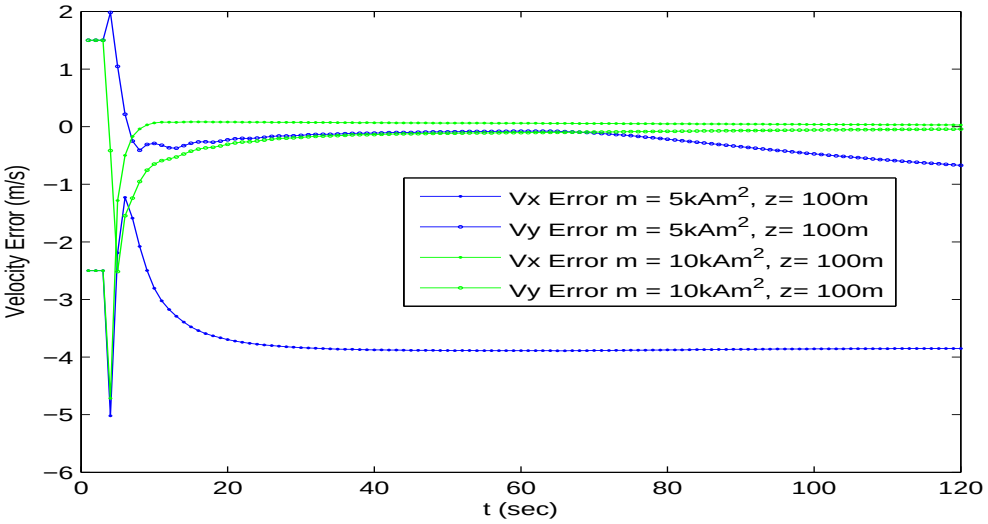

(a) Velocity tracking

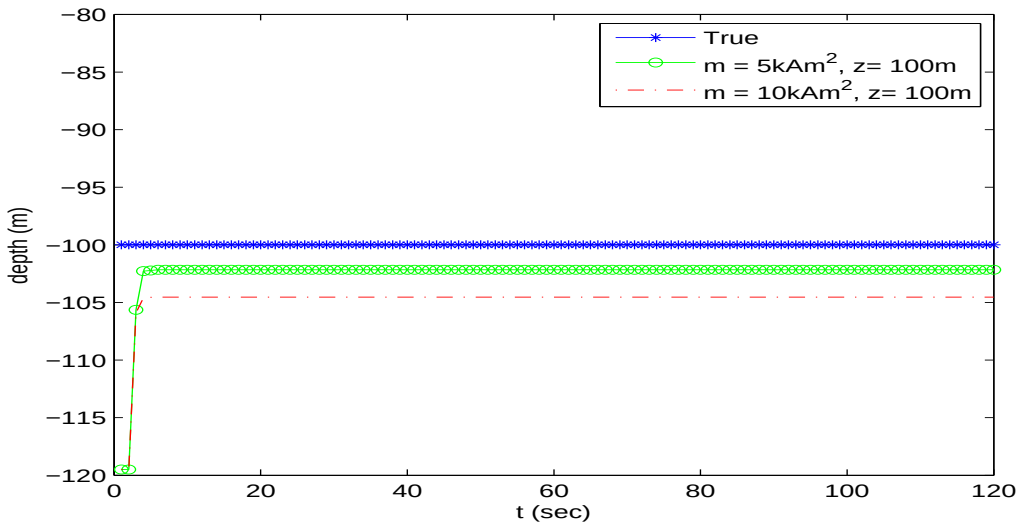

(b) Depth tracking

Figure 5.21: Performances in Velocity Tracking and Depth Localisation Considering Range of Detection

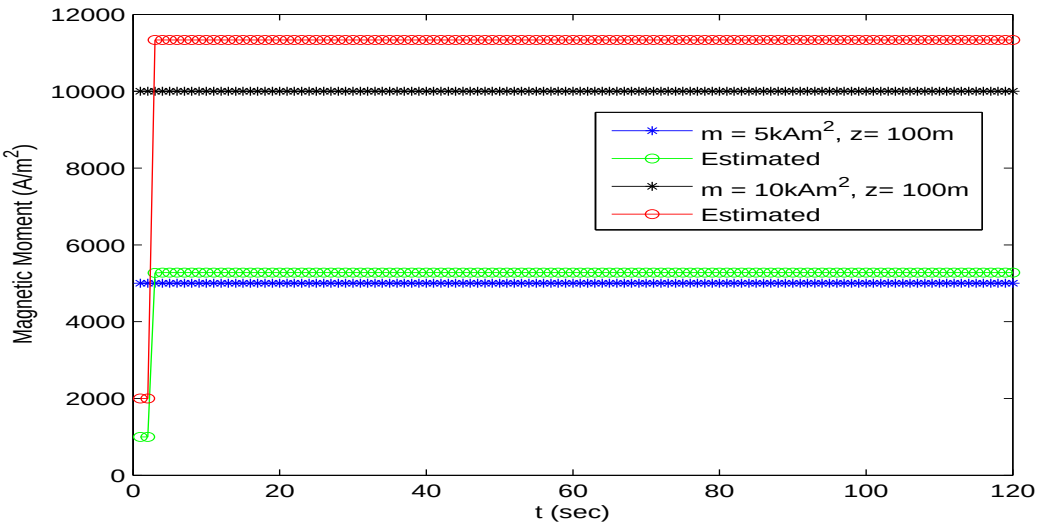

(a) Magnetic moment estimation

Figure 5.22: Performances in Classification Considering Range of Detection

Chapter 6

CONCLUSION AND FUTURE WORKS

This study presents a method for underwater surveillance system which requires detection, classification, localization and tracking of a ferromagnetic object from noisy magnetic field measurements involving the modeling of a non-linear system.

The fields computation model in a stratified media along with modeling of target magnetization and multiple noise sources placement in global coordinate system are very elegant techniques for designing a magnetic signals measurement system. A MAD system observes noisy magnetic signals, and responds to any anomaly found in the recorded signals. EMD method is used to decompose the noisy signals into IMFs and residue, and detect the anomaly produced by the target from dominant IMFs ignoring the noise contributions.

We also investigated the possibility of using combined PF and UKF for classification, localisation and tracking of a target modeled as an equivalent magnetic dipole of arbitrary size, velocity and trajectory. The problem is formulated in state-space form where the state parameters are the magnetic moment, position and velocity of the target. Because of the non-linearity of the observation equation, to solve this problem it is necessary to use various approximations. UKF is best suited for non-linear dynamic systems but the unknown arrival directions and arbitrary

initial state values make unsatisfactory results. On the other hand PF requires several times longer execution period, and ignores most recent measurement, which also not acceptable for continuous monitoring phenomena of this problem. So, Triangular 3-sensors and Pyramid 5-sensors systems used for this application are to cover the possible directions of arrival, and the use of PF is for the flexibility in selecting the initial state parameters which updates the states for the UKF. All the target parameters like the position, velocity, and equivalent magnetic moments are estimated with a good level of accuracy by the proposed method.

The topics studied in this thesis are very challenging in recent time. The following parts of the problem are still open for future works:

- More details modeling of each of noise sources like modeling of ocean internal and surface waves, solar irradiation, complex flow pattern of water, sea floor wreckages etc., are necessary for measuring magnetic noise for more real like air-ocean environments.

- Improvement and modifications are required for detecting two or more targets simultaneously from low SNR signals.

- More investigations are required for optimal sensor geometry for very small to very large target classification, and for velocity having acceleration (turnover maneuver).

- Doppler effects must be in consideration for observations of MAD systems that involves Doppler shifts due to relative motions of noise sources, target, and UAV.

- Real Field tests are necessary for determining both the Range of Detection (the

distance between the magnetic sensor and the target) and the Probability of Detection (Pd).

Bibliography

[1] Enric G., Vladimir D., Marc C., David P. W., "A Real-time Underwater Object Detection Algorithm for Multi-beam Forward Looking Sonar", IFAC Proceedings Volumes, Volume 45, Issue 5, Pages 306-311, ISSN 1474-6670, 2012.

[2] Ruiz I. T., Petillot Y.,Lane D. and Bell J., "Tracking objects in underwater multibeam sonar images," IEE Colloquium on Motion Analysis and Tracking (Ref. No. 1999/103), pp. 11/1-11/7 London, 1999.

[3] Pailhas, Y., and Petillot, Y., "Large MIMO sonar systems: A tool for underwater surveillance," Sensor Signal Processing for Defence (SSPD), Edinburgh, pp. 1-5. 2014.

[4] Dill, T.J., "Modeling the Performance of a Laser for Tracking an Underwater Dynamic Target" Doctoral dissertation, Florida Atlantic University, 2014.

[5] Caimi, F.M., Kocak, D.M., Dalgleish, F. and Watson, J., "Underwater imaging and optics: Recent advances" In OCEANS 2008 (pp. 1-9). IEEE, 2008.

[6] Hohle, J. "Reconstruction of the Underwater Object Photogramm" Eng. Remote Sens. 37, 948954, 1971.

[7] Holmes, J.J., "Exploitation of a ship's magnetic field signatures", Synthesis Lectures on Computational Electromagnetics, 1(1), pp.1-78, 2006.

[8] Sanford, T. B., Motionally induced electric and magnetic fields in the sea, J. Geophys. Res., Vol. 76(15), pp. 34763492, 1971.

[9] Podney, W., Electromagnetic fields generated by ocean waves, J. Geophys. Res., vol. 80(21), pp. 29772990, 1975.

[10] Avera, W. E., Gallacher, P. C., Teague, W. J., Liang, R., and Nelson, J. B., "Magnetic noise associated with ocean internal waves," OCEANS 2009, Biloxi, MS, pp. 1-4, 2009.

[11] Manoj, C., Kuvshinov, A., Maus, S. et al, "Ocean circulation generated magnetic signals". Earth Planet Sp (2006), vol 58, pp. 429-437, 2006.

[12] British Geological Society "The Earth's Magnetic Field: An Overview". Available: `http://www.geomag.bgs.ac.uk/education/earthmag.html` [Last online accessed: 2017-05-04].

[13] Ginzburg, B., Frumkis, L., Kaplan, B.Z., Sheinker, A. and Salomonski, N.,"Investigation of advanced data processing technique in magnetic anomaly detection systems", Int. J. Smart Sens. Intell. Ststems, Vol 1, pp.110-122, 2008.

[14] Sheinker, A., Frumkis, L., Ginzburg, B., Salomonski, N., and Kaplan, B. Z., "Magnetic Anomaly Detection Using a Three-Axis Magnetometer," in IEEE Transactions on Magnetics, vol. 45, no. 1, pp. 160-167, Jan. 2009.

[15] Yvinec, Y., Druyts, P., and Dupont, Y., "Detection and Classification of Underwater Targets by Magnetic Gradiometry" in Proceedings of International Conference on Underwater Remote Sensing, 2012.

[16] Nimisha V., "Iterative Denoising of Geophysical Time Series Using Wavelets", 5th Conference & Exposition on Petroleum Geophysics, Hyderabad, India PP 943-947, 2004.

[17] Xiong L., Understanding 3D analytic signal amplitude. GEOPHYSICS, 71(2), L13-L16, 2006.

[18] Roest, W. E., Verhoef, J., and Pilkington, M., "Magnetic interpretation using the 3-D analytic signal" Geophysics, 57, 116, 1992.

[19] Reid, A. B., Allsop, J. M., Granser, H., Millet, A. J., and Somerton, I. W., "Magnetic interpretation in three dimensions using Euler deconvolution" Geophysics 55, 1, 80, 1990.

[20] Changhan, X., Shengdao, L., and Guo-hua, Z., "Real-time localization of a magnetic object with total field data" Automation Congress, 2008. WAC 2008. World 2008.

[21] Fan, L., Kang, C., Zhang, X., Zheng, Q., and Wang, M., "An efficient method for tracking a magnetic target using scalar magnetometer array" SpringerPlus, vol. 5(1), p.502, 2016.

[22] Francisco, C. T., and Antonio, P., "Magnetic Navigation and Tracking of Underwater Vehicles", IFAC Proceedings Volumes, Volume 46, Issue 33, Pages 239-244, 2013.

[23] Niu, J., Teng, B., and Yin, W., "Investigation on the Real-Time Tracking of Single Magnetic Target under the Geomagnetic Background" Appl. Math, vol. 6(1S), pp.41S-46S, 2012.

[24] Abdelrahman, E.M., and Essa, K.S., A new method for depth and shape determinations from magnetic data" Pure and Applied Geophysics, vol. 172(2), pp.439-460, 2015.

[25] Young, J. A., and Clark, D. A., "Magnetic tensor gradiometry in the marine environment," International Conference on Electromagnetics in Advanced Applications, Sydney, NSW, 2010, pp. 701-704, 2010.

[26] Tang, C.M., "Electromagnetic fields due to dipole antennas embedded in stratified anisotropic media," in IEEE Transactions on Antennas and Propagation, vol. 27, no. 5, pp. 665-670, Sep 1979.

[27] Kong, J.A., "Electromagnetic fields due to dipole antennas over stratified anisotropic media", Geophysics, 37(6), pp.985-996, 1972.

[28] Winckel, G.V., "Legendre-gauss quadrature weights and nodes,", Available: http://www.mathworks.com/matlabcentral/fileexchange/4540-legendre-gauss-quadrature-weights-and-nodes, [last online access: 2016-04-29], 2004.

[29] X.B. Xu and L. Zeng, "Ferromagnetic Cylinders in Earth's Magnetic Field-a Two-Dimentional Model of Magnetization of Submarine" Journal Of Electromagnetic Waves And Applications Vol. 12 , Iss. 10,1998.

[30] S. Aditya. (2015, August 15). Denoising signals using empirical mode decomposition and hurst analysis, Available: https://www.mathworks.com/matlabcentral/fileexchange/52502-denoising-signals-using-empirical-mode-decomposition-and-hurst-analysis, [Last online accessed: 2016-11-28], 2015.

[31] Diego Andrs Alvarez Marn (2012, 14 August). Particle filter tutorial, Available: https://www.mathworks.com/matlabcentral/fileexchange/35468-particle-filter-tutorial, [Last online accessed: 2017-05-21]., 2012.

[32] J. J Simon; M. Rudolph van der. (2000, August 14). UNSCENTED KALMAN FILTER, Available: http://www.cs.cmu.edu/afs/cs/Web/People/motionplanning/papers/sbp_papers/kalman/ukf/ukf.m, [Last online accessed: 2016-11-28], 2000.